

1  
2  
3  
4  
5  
6  
7  
8  
9  
10  
11  
12  
13  
14  
15  
16  
17  
18  
19  
20  
21  
22  
23  
24  
25  
26  
27  
28  
29  
30  
31  
32

# Development and Evaluation of the Aerosol Forecast Member in NCEP's Global Ensemble Forecast System (GEFS-Aerosols v1)

Li Zhang<sup>1,2</sup>, Raffaele Montuoro<sup>1,2</sup>, Stuart A. McKeen<sup>1,3</sup>, Barry Baker<sup>4,5</sup>, Partha S. Bhattacharjee<sup>6</sup>, Georg A. Grell<sup>2</sup>, Judy Henderson<sup>2</sup>, Li Pan<sup>6</sup>, Gregory J. Frost<sup>3</sup>, Jeff McQueen<sup>7</sup>, Rick Saylor<sup>8</sup>, Haiqin Li<sup>1,2</sup>, Ravan Ahmadov<sup>1,2</sup>, Jun Wang<sup>7</sup>, Ivanka Stajner<sup>7</sup>, Shobha Kondragunta<sup>9</sup>, Xiaoyang Zhang<sup>10</sup>, Fangjun Li<sup>10</sup>

<sup>1</sup>*CIRES, University of Colorado, Boulder, CO, US;*

<sup>2</sup>*Global Systems Laboratory, Earth System Research Laboratory, NOAA, Boulder, CO, US;*

<sup>3</sup>*Chemical Sciences Laboratory, Earth System Research Laboratory, NOAA, Boulder, CO, US;*

<sup>4</sup>*NOAA Air Resources Laboratory, College Park, MD, US;*

<sup>5</sup>*Cooperative Institute for Climate and Satellites, University of Maryland, College Park, MD, US;*

<sup>6</sup>*I.M. Systems Group at NCEP/NWS/EMC, College Park, MD, US;*

<sup>7</sup>*Environmental Modeling Center, National Weather Service, Greenbelt, MD, US;*

<sup>8</sup>*NOAA Air Resources Laboratory, Oak Ridge, TN, US;*

<sup>9</sup>*NOAA/NESDIS Center for Satellite Applications and Research, Greenbelt, MD, US;*

<sup>10</sup>*Department of Geography, South Dakota State University, Brookings, SD, US*

Submit to Geoscientific Model Development

May 2022

\*Correspondence to: Li Zhang ([kate.zhang@noaa.gov](mailto:kate.zhang@noaa.gov))

CIRES, University of Colorado Boulder

GSL EPAD, NOAA ESRL

325 Broadway David Skaggs Research Center R/GSL1

Boulder, CO 80305

1-303-497-3956

1 **Abstract.**

2 NOAA's National Weather Service (NWS) is on its way to deploy various operational prediction applications using the  
3 Unified Forecast System (<https://ufsccommunity.org/>), a community-based coupled, comprehensive Earth modeling system.  
4 An aerosol model component developed in a collaboration between the Global Systems Laboratory, Chemical Science  
5 Laboratory, the Air Resources Laboratory, and Environmental Modeling Center (GSL, CSL, ARL, EMC) was coupled  
6 online with the FV3 Global Forecast System (FV3GFS) using the National Unified Operational Prediction Capability  
7 (NUOPC)-based NOAA Environmental Modeling System (NEMS) software framework. This aerosol prediction system  
8 replaced the NEMS GFS Aerosol Component version 2 (NGACv2) system in the National Center for Environment  
9 Prediction (NCEP) production suite in September 2020 as one of the ensemble members of the Global Ensemble Forecast  
10 System (GEFS), dubbed GEFS-Aerosols v1. The aerosol component of atmospheric composition in GEFS is based on the  
11 Weather Research and Forecasting model (WRF-Chem). GEFS-Aerosols includes bulk modules from the Goddard  
12 Chemistry Aerosol Radiation and Transport model (GOCART). Additionally, the biomass burning plume rise module from  
13 High-Resolution Rapid Refresh (HRRR)-Smoke based on WRF-Chem was implemented; the GOCART dust scheme was  
14 replaced by the FENGSHA dust scheme (developed by ARL); the Blended Global Biomass Burning Emissions Product  
15 (GBBEPx version 3) provides biomass burning emission and Fire Radiative Power (FRP) data; and the global anthropogenic  
16 emission inventories are derived from the Community Emissions Data System (CEDS). All sub-grid scale transport and  
17 deposition is handled inside the atmospheric physics routines, which required consistent implementation of positive definite  
18 tracer transport and wet scavenging in the physics parameterizations used by NCEP's operational Global Forecast System  
19 based on FV3 (FV3GFS). This paper describes the details of GEFS-Aerosols model development and evaluation of real-time  
20 and retrospective runs using different observations from in situ measurement, satellite and aircraft data. GEFS-Aerosols  
21 predictions demonstrate substantial improvements for both composition and variability of aerosol distributions over those  
22 from the former operational NGACv2 system with the fundamental updates (e.g. dust and fire emission) in atmospheric and  
23 chemical transport model.

24

25

26

## 1 **1. Introduction**

2 The operational air quality predictions in National Oceanic and Atmospheric Administration (NOAA)'s National Weather  
3 Service (NWS) contribute to the protection of lives and health in the US (<https://airquality.weather.gov>). These predictions  
4 are used by state and local air quality forecasters to issue official air quality forecasts for their respective areas. The U.S.  
5 Environmental Protection Agency (EPA) and the Centers for Disease Control and Prevention (CDC) also use the NOAA  
6 forecasts for applications with wildfire, health and smoke vulnerability assessments. Exposure to fine particulate matter, i.e.,  
7 aerosol particles with diameters of 2.5  $\mu\text{m}$  and smaller ( $\text{PM}_{2.5}$ ), is recognized as a major health concern and the associated  
8 mortality rate is estimated to be higher than the five specific causes of death examined by the global burden of disease [GBD,  
9 Burnett et al., 2018].

10 It is well known that the role of aerosols in Numerical Weather Prediction (NWP), through interaction with atmospheric  
11 radiation and precipitation physics (direct, semidirect, and indirect effect), and their impact on meteorological fields in both  
12 weather and climate scale, have been widely recognized in many studies [e.g. Fast et al. 2006, Levin and Cotton, 2009;  
13 Chen et al., 2011; Grell et al. 2011; Forkel et al. 2012; Muhlbauer et al., 2013; Xie et al., 2013; Yang et al., 2014; Wang H.  
14 et al., 2014, Wang Q. et al., 2014]. Additional studies at operational weather centers indicate the importance of including  
15 aerosol feedback in NWP for operational forecasting [Rodwell and Jung, 2008; Reale et al., 2011; Mulcahy et al., 2014;  
16 Bozzo et al, 2020]. At National Centers for Environmental Prediction (NCEP), the operational RAPid refresh (RAP) and  
17 High-Resolution Rapid Refresh (HRRR) storm scale modeling systems now include the impact of aerosols from biomass  
18 burning emissions on radiation. Due to the importance of aerosol feedback in NWP, the performance of predicted aerosols  
19 and their optical properties are critical before implementing the aerosol direct and semi-direct effect in NWP.

20 Since last decade, global aerosol modeling grows rapidly to provide operational prediction and air quality alters in NWP.  
21 More than 15 years ago, NASA implemented an aerosol transport module, Goddard Chemistry Aerosol Radiation and  
22 Transport model (GOCART), online within the its Global Modeling and Assimilation Office (GMAO) Goddard Earth  
23 Observing System version 4 (GEOS-4) atmospheric general circulation model (AGCM) [Bloom et al., 2005], which is able  
24 to run in climate, data assimilation and replay modes [Colarco, et al., 2010]. Later on, it switched to the next version of  
25 GEOS-5 to provide near-real time forecast of aerosols and atmospheric compositions [Rienecker et al., 2008; Molod et al.,  
26 2015]. Since 2008, as part of the project Global and regional Earth-system Monitoring using Satellite and in situ data  
27 (GEMS) the European Centre for Medium-Range Weather Forecasts (ECMWF) began to provide aerosol forecast  
28 [Hollingsworth et al., 2008; Morcrette et al., 2009; Benedetti et al. 2009]. In 2010, the International Cooperative for Aerosol  
29 Prediction (ICAP) was founded with one of its goals being the development of a global multi-model aerosol forecasting  
30 ensemble (ICAP-MME) for basic research and eventual operational use [Benedetti et al., 2011; Reid et al., 2011; Colarco et  
31 al., 2014]. In the ICAP, the complete aerosol forecast models are original from European Centre Medium Range Weather  
32 Forecasts Copernicus Atmosphere Monitoring Service (ECMWF-CAMS), the Japan Meteorological Agency Model of  
33 Aerosol species in the Global Atmosphere (JMA-MASINGAR), the National Aeronautics and Space Administration (NASA)

1 Goddard Earth Observing System Version 5 (NASA-GEOS-5) and the Naval Research Lab Navy Aerosol Analysis and  
2 Prediction System (NRL-NAAPS) modeling systems. There are also dust Dust-only model from the Barcelona  
3 Supercomputer Center Chemical Transport Model (NMMB/BSC-CTM), the United Kingdom Met Office Unified Model  
4 (UKMO-UM) and National Oceanic and Atmospheric Administration/National Centers for Environmental Prediction  
5 (NOAA NCEP) Environmental Modeling System (NEMS) Global Forecast System (GFS) Aerosol Component (NGAC)  
6 [Sessions et al., 2015]. Xian et al. [2019] summarized and compared the current states and performances of these global  
7 operational aerosol model in ICAP. The aerosol feedback is no included into these operational models, and they are mostly  
8 driven by independent operational/quasi-operational meteorological models developed at different NWP/research center with  
9 different vertical and horizontal resolution. All these models include the major aerosol species of black carbon (BC), organic  
10 carbon (OC), sulfate, sea salt and dust, GEOS-5 has extra trace of nitrate. The AOD root mean square error (RMSE) between  
11 ICAP-MME and 21 representative sites of AERONET from 2012 to 2017 indicates improvements for find-mode AOD,  
12 while it shows small signals of potential model improvement over the regions where is impacted by the biomass burning  
13 emission and dust [Xian et al., 2019].

14 NCEP, in collaboration with the NASA/Goddard Space Flight Center (GSFC), developed the NEMS Global Forecast System  
15 (GFS) Aerosol Component version 1 (NGACv1) for predicting the distribution of global atmospheric aerosols [Lu et al.,  
16 2010]. NGAC is an interactive atmospheric aerosol forecast system with the NEMS global spectral model (NEMS GSM) as  
17 the atmosphere model and GOCART as the aerosol model [Wang et al., 2018]. NGACv1 was implemented in 2012 and  
18 provided the first operational global dust aerosol forecasting capability at NCEP [Lu et al., 2016]. In NGACv1 an in-line  
19 aerosol module based on the Goddard Chemistry Aerosol Radiation and Transport (GOCART) model from GEOS-5 [Chin et  
20 al., 2000], but limited to dust only, was used. The NGACv1 used the Earth System Modeling Framework (ESMF) to couple  
21 the aerosol module with the GFS. Later, NCEP implemented a multispecies aerosol forecast capability NGACv2, based on  
22 NGACv1 through collaborations among NCEP, NASA/GSFC, the NESDIS Center for Satellite Applications and Research  
23 (STAR), and the State University of New York at Albany [Wang et al., 2018].

24 In July 2016, NOAA took a significant step toward developing a state-of-the-art global weather forecasting model by  
25 announcing the selection of a new dynamic core developed at NOAA Geophysical Fluid Dynamics Laboratory (GFDL) to  
26 upgrade the GFS. The GFDL Finite-Volume Cubed-Sphere Dynamical Core (FV3) replaced the spectral GFS core in June of  
27 2019 to drive global NWP systems with improved forecasts of severe weather, winter storms, and tropical cyclone intensity  
28 and track. NOAA is now on the way to integrate various operational applications into the Unified Forecast System (UFS), a  
29 comprehensive, community-based coupled Earth modeling system, designed as both a research tool and the basis for NOAA  
30 operational forecasting applications.

31 Here we describe a new aerosol model component developed through collaborative efforts among the Global Systems  
32 Laboratory (GSL), the Chemical Science Laboratory (CSL), and the Air Resources Laboratory (ARL), Environmental  
33 Modeling center (EMC) and STAR. This aerosol component was implemented operationally on September 2020 to provide  
34 five-day global aerosol forecasts with  $\sim 25$  km horizontal resolution and 64 vertical layers from the surface to 0.2 hPa as one

1 member of the Global Ensemble Forecast System of version 12 (GEFSv12): GEFS-Aerosols v1. The aerosol component is  
2 designed as an independent model component for the NOAA Environmental Modeling System (NEMS) framework and  
3 includes a coupling interface based on the National Unified Operational Prediction Capability (NUOPC) Layer for model  
4 interoperability. All chemistry, aerosol, and emission modeling processes reside and run within this model component. There  
5 is not aerosol feedback on the atmospheric model of GEFS, and the aerosols are not in any way interactive with the radiation  
6 and clouds. GEFS-Aerosols shows a substantial improvement for both composition and variability of aerosol distributions  
7 over those from the previous global aerosol prediction system NGACv2. The model predicted global aerosol products from  
8 GEFS-Aerosols are also used for other applications, such as to provide lateral boundary conditions for NOAA's regional  
9 National Air Quality Forecast Capability (NAQFC), satellite sea surface temperature (SST) physical retrievals, and the  
10 global solar insolation estimation [Wang et al., 2018].

11 The current study presents the development of GEFS-Aerosols and evaluations of its performance in real time and  
12 retrospective experiments. Section 2 describes the coupling components of the GEFS-Aerosols member, including the  
13 atmospheric component of FV3GFS model, the aerosol component, and the observation, reanalysis, and model data used for  
14 evaluation and comparison. The emission inventories of both anthropogenic emission and biomass burning emissions and  
15 other chemical input data are presented in Section 3. Section 4 and Section 5 are the evaluations of Day-1 real-time forecast  
16 since July 2019 and the Day-1 retrospective forecast for the ATom-1 periods of 2016 summer, respectively. The conclusions  
17 and future plans are summarized in Section 6.

## 18 **2. Model and data**

### 19 **2.1 Descriptions of GEFS-Aerosols**

#### 20 **2.1.1 FV3GFS and GEFS-Aerosols**

21 The global Finite-Volume cubed-sphere dynamical core (FV3) developed by GFDL was chosen by NOAA as the non-  
22 hydrostatic dynamical core to be the Next Generation Global Prediction System (NGGPS) of the National Weather Service  
23 in the US [Black et al., 2021]. Currently, the FV3 was successfully implemented within the physical scheme of GFS version  
24 15 (named as FV3GFS v15), which became operational on June 2019. It has the capability to provide the metrological basis  
25 for coupling with aerosol prediction component. The GEFS is a weather forecast modeling system made up of 31 separate  
26 forecasts, or ensemble members, which have the same horizontal (~25 km) and vertical resolution (64 layers from the  
27 surface to 0.2 hPa). The GEFS-Aerosols model is only using one of the same weather model as other GEFS members except  
28 it includes the prognostic aerosols from the coupling aerosol component. The NCEP started the GEFS to address the nature  
29 of uncertainty in weather observations that are used to initialize weather forecast models and uncertainties in model  
30 representation of atmospheric dynamics and physics. The aerosol component coupled with FV3GFS v15 has been merged

1 into the GEFS, as a single ensemble member named as GEFS-Aerosols, for real-time and retrospective forecast that  
2 preceded operational implementation, which occurred in September 2020.

3 In GFS v15, all sub-grid scale transport and convective deposition related to aerosol is handled inside the atmospheric  
4 physics routines of simplified Arakawa–Schubert (SAS) scheme. It requires consistent implementation of positive definite  
5 tracer transport and wet scavenging in the physics parameterizations, which was implemented subsequent in the forecast  
6 system of GEFSv12.

### 7 **2.1.2 Aerosol component**

8 The current aerosol component in the GEFS-Aerosols model is based on the simple bulk aerosol modules from WRF-Chem  
9 [Grell et al., 2005; Powers et al., 2017], and the first time to be used in the global model is the Flow-following finite-volume  
10 Icosahedral Model (FIM), as FIM-Chem [Zhang et al, 2022], including aerosol modules from GOCART. The metrological  
11 fields (such as land use and other climatological surface fields, vegetation type etc.) are imported from the FV3 atmospheric  
12 model to the chemical model to drive the aerosols components. They are consistent in the FV3 atmospheric model and  
13 chemical model. Other than the aerosols convective wet scavenging, all the chemical related processes of source and sink,  
14 such as emission, dry deposition, settling, large-scale wet deposition, chemical reactions are handled by the chemical model.  
15 The large-scale wet deposition and dry deposition modules are from WRF-Chem for GOCART aerosols scheme, which are  
16 column model driven by meteorological input from atmospheric model. Large-scale wet removal of aerosols includes below-  
17 cloud removal (washout) following Easter et al. [2004] and the details of below-cloud wet scavenging via interception and  
18 impaction can be found in Slinn [1984]. The dry deposition is the same as Chin et al. [2002]. After updating the chemical  
19 tracers in chemical model, they are passed back to FV3 atmospheric model for transport and advection.

20 The GOCART aerosol modules use simplified sulfur chemistry for sulfate simulation, bulk aerosols of BC, OC, and  
21 sectional dust and sea salt [Chin et al., 2000]. For OC and BC, the hydrophilic and hydrophobic components are considered  
22 and the chemical reactions for gaseous sulfur oxidations are calculated using prescribed OH, H<sub>2</sub>O<sub>2</sub>, and NO<sub>3</sub> fields for  
23 gaseous sulfur oxidations [Chin et al., 2000]. The GOCART model background fields of prescribed OH, H<sub>2</sub>O<sub>2</sub>, and NO<sub>3</sub>  
24 have been replaced by the newer version of 2015 from the NASA GEOS Global Modeling Initiative (GMI) Chemical  
25 transport model (<https://acd-ext.gsfc.nasa.gov/Projects/GEOSCCM/MERRA2GMI/>). These are monthly mean data and these  
26 prescribed OH, H<sub>2</sub>O<sub>2</sub>, and NO<sub>3</sub> fields would not be transported and changed in space. The marine dimethyl sulfide (DMS)  
27 emission is calculated as a product of sea water DMS concentration and sea-to-air transfer velocity as described by Chin et  
28 al., [2000]. Recently, some modifications and updates have been implemented, including the biomass burning plume rise  
29 module adapted from High-Resolution Rapid Refresh (HRRR)-Smoke based on WRF-Chem, the capabilities of using the  
30 version 3 biomass-burning emission calculations based on the Blended Global Biomass Burning Emissions Product  
31 (GBBEPx, Zhang et al., 2014] and Fire Radiative Power (FRP) data provided by NESDIS (GBBEPx v3) as well as the  
32 application of the global anthropogenic emission inventories from Community Emissions Data System (CEDS).

1 The sea salt scheme was updated to the most recent version with five size bins based on NASA's 2nd-generation GOCART  
2 model (Colarco et al., 2010). The model has the capability of handling volcanic eruptions, which need the estimate of  
3 injection height and SO<sub>2</sub> and volcanic ash emissions. While for the predicted results in the paper, the volcanic emission has  
4 not been included.

5 A new dust emission scheme, referred to as FENGSHA, was implemented in GEFS-Aerosols. The scheme, which is also  
6 used in NOAA's National Air Quality Forecast Capability, is modified from the original Owen equation [Tong et al., 2017,  
7 Owen, 1964; Shao et al., 1993],

$$8 \quad F = \sum_{j=1}^N K \times A \times \frac{\rho}{g} \times S \times u_* \times (u_*^2 - u_{*tj}^2) \quad \text{for } u_* > u_{*tj} \quad (1)$$

9 where  $N$  is the number of soil types in a particular grid cell,  $K$  is the ratio of vertical to horizontal emission flux,  $A$  represents  
10 particle supply limitation (availability),  $\rho$  is air density,  $g$  is gravitational acceleration,  $S$  is the soil erodibility potential,  $u_*$  is  
11 friction velocity, and  $u_{*tj}$  is the threshold friction velocity for soil type  $j$  [Shao et al., 1993]. Dust emission is calculated only  
12 when friction velocity exceeds the designated threshold value for the land use type and soil texture. The threshold friction  
13 velocities are based on wind tunnel measurements done in both the laboratory and field [Gillette et al., 1980].

14 What makes FENGSHA unique is the way in which the threshold values are determined. Unlike models based on  
15 Marticorena and Bergametti [1995] or Shao et al., [2011], threshold values are based on surface and wind tunnel flux  
16 measurements of saltation [Gillette, 1988]. The drag partition in the FENSGHA scheme is described by the MacKinnon et al.  
17 [2004] parametrization using the model surface roughness ( $z_0$ ) or derived from the surface roughness estimates using the  
18 Advanced Scatterometer (ASCAT) as described by Prigent et al. [2012]. The Fécan et al [1998] soil moisture correction is  
19 used to adjust the dry threshold friction velocity. Once the total windblown dust emission flux is computed the total flux is  
20 distributed into the modeled dust bins using the Kok [2011] distribution.

21 A new sediment supply map, the Baker-Schepanski Map (BSM), which was developed from the ideas of Chappell and  
22 Webb [2016] is currently used within the GEFS-Aerosol FENGSHA implementation. Chappell and Webb [2016] created an  
23 approach similar to that of the Raupach [1992] model for lateral cover but instead uses a top-down view to describe the area  
24 of the turbulent wake using an analogous shadow instead of a two-dimensional view. The shadow approach is sensitive to  
25 the configuration of the roughness elements meaning that it is sensitive to the placement of the roughness elements in  
26 relation to each other. The BSM describes the probability of momentum mixing directly to the soil surface through the  
27 canopy. For the application into GEFS-Aerosols a monthly 3-year climatology of the BSM was created which refers to a  
28 monthly average over 3 observation years, in this case 2016, 2017 and 2018 as these were the latest full years at the time of  
29 model development.

### 30 **2.1.3 GEFS-Aerosols coupled architecture, running sequence and forecasting workflow**

1 The aerosol component of GEFS-Aerosols couples directly to the FV3-based atmospheric component via the NUOPC Layer  
2 [Theurich et al., 2016], which is the foundation of NOAA’s modeling framework (Fig. 1). Fig. 2a shows the model coupled  
3 structure that the aerosol component imports meteorological fields from the atmospheric model and exchanges aerosol  
4 mixing ratios at each coupling time step via standard NUOPC connectors. Each aerosol species is simulated as a prognostic  
5 atmospheric tracer, which is advected by the FV3 dynamical core and undergoes convective mixing and PBL diffusion  
6 within the atmospheric physics. All aerosol composition and emission-related processes are computed in GEFS-Aerosols  
7 after the atmospheric physics has been advanced and passed to the chemical model following the sequences as emission,  
8 settling of dust and sea salt, plume-rise of fire emission, dry deposition, large-scale wet deposition, chemical reactions and  
9 carbonaceous aerosol updating. Tracer mixing ratios are then updated and exported back to the atmospheric model.

10 Bundling all aerosol composition processes in a single model component led to the implementation of a sequential coupling  
11 scheme with the atmospheric component. At each coupling time step, the atmospheric dynamical core and physics processes  
12 (including radiation) are computed first. The aerosol component is then executed to perform all air composition processes  
13 and transfer the updated tracers back to the atmospheric component. Finally control returns to the atmospheric model, which  
14 updates the atmospheric state with new meteorology and aerosols concentrations. To minimize overhead associated with  
15 data exchange between model components, GEFS-Aerosols is run on the atmospheric grid, which is imported from the  
16 atmospheric component through NUOPC. Additionally, the coupling run sequence assigns to the aerosol component the  
17 identical set of Persistent Execution Threads (PETs) used by the atmospheric model’s forecast component. This allows the  
18 model to leverage NUOPC’s ability to access coupling fields by memory reference, minimizing the memory footprint for the  
19 coupled system.

20 The sequence of steps involved in moving from the beginning to the end of a forecast process is controlled by the workflow.  
21 In a retrospective or real time forecast, the chemical tracers are cycled from the output of a previous forecast as the initial  
22 condition. In operation, the computational cost with aerosol component would take 129 mins for 120 hours forecast.  
23 Therefore, the efficiency is about 2.53 times computational cost by including aerosol component compared to the one  
24 without aerosol component in the forecast. In the operation, there is no execution time by including the aerosols component  
25 as one of the ensemble members since this member only performs 120 hours forecast by including aerosol component, which  
26 is shorter than other members without aerosol component that perform 384 hours forecast.

27 The workflow shown in Figure 2(b) describes the steps including pre-processing (prepare input data) and post-processing  
28 (process output data) before and after forecast for the GEFS-Aerosols in the forecast system. This initial implementation of  
29 GEFS-Aerosols does not include aerosol data assimilation, so the chemical tracers in the restart files are used as the chemical  
30 initial condition for the next forecast. The yellow box includes the tasks/steps for atmospheric mode, while the green box  
31 includes the tasks/steps for chemical model. The AOD is calculated in the post-processing part of the workflow, using a  
32 look-up table (LUT) of aerosol optical properties from NASA GOCART model [Colarco et al. 2010, Colarco et al. 2014],  
33 which was implemented in the Unified Post Processor (UPP, <https://dtcenter.org/community-code/unified-post-processor->



1 upp). It should be noted that the LUT reflects the impacts of a larger number of aerosol species in the atmosphere than the  
2 simple GOCART module treats. Also, considering the bulk aerosol scheme in GOCART, there is no size distribution for OC,  
3 BC and sulfate, the LUT may have uncertainties in the AOD calculation. Based on observational validation, some  
4 adjustments have been applied in into LUT calculation to compensate the contributions for the absence of nitrate,  
5 ammonium and secondary organic aerosol (SOA) in GOCART.

## 6 **2.2 Observation, reanalysis data and other model data**

7 The real-time forecast experiments were evaluated using the following ensemble analysis, reanalysis data, satellite and in  
8 situ observational data, aircraft measurements, and model predictions. We compare each day model forecast hours with same  
9 day reanalysis or analysis data and compute the AOD statistics (e.g. bias, RMSE, correlation etc.) for each grid for each pair  
10 of model and reanalysis or analysis data for that model forecast hour. We then calculate that for the entire 4 months of the  
11 study period and averaged it over the entire 4 months for each grid points. This method gives an overall estimate  
12 of systematic bias of the model in spatial and temporal scale.

### 13 2.2.1 Reanalysis data of AOD

14 1) Total AOD instantaneous reanalysis dataset from the second Modern-Era Retrospective analysis for Research and  
15 Application [MERRA-2, Gelaro et al., 2017]. The MERRA-2 reanalysis provides various AOD product at  $0.625 \times$   
16  $0.5$  degree horizontal resolution and at 72 vertical levels. MERRA-2 reanalysis data is not synchronous as real-time,  
17 and normally has 1-2 months' time lag.

### 18 2.2.2 Observation data of Satellite AOD, AERONET AOD and ATOM-1 concentration.

19 1) MODIS provides near-global coverage of aerosol measurements in space and time. We have used a MODIS Level-  
20 3 (daily and monthly at 1 degree horizontal resolution) AOD dataset in this study  
21 (<https://ladsweb.nascom.nasa.gov/>). The dataset belongs to the Collection 6.1 combined land and ocean from the  
22 Aqua satellite [Levy et al., 2013]. This latest collection of MODIS data includes AOT data based on refined  
23 retrieval algorithms, in particular the expanded Deep Blue algorithm [Hsu et al., 2013; Sayer et al., 2013]. It  
24 introduces a merged AOD product, combining retrievals from the Dark Target (DT) and Deep Blue (DB)  
25 algorithms to produce a consistent data set covering a multitude of surface types ranging from oceans to bright  
26 deserts [Sayer et al., 2014]. In this work the aerosol product `Dark_Target_Deep_Blue_Combined_Mean` was used  
27 for quantitative evaluation of model results. We have used Collection 6.1 MODIS AOD at 550nm, which has  
28 Expected Errors (EEs) of  $[\pm (0.05 + 15\%AOD)]$  and  $[\pm (0.03 + 5\%AOD)]$  for Dark Target retrievals at a 10-km  
29 resolution over land and ocean, respectively. The EEs are approximately  $[\pm (0.03+21\%AOD)]$  for 'arid' and  $[\pm$   
30  $(0.03+18\%AOD)]$  for 'vegetated' path Deep Blue retrievals at a 10-km resolution over land [Levy et la., 2013].  
31 2) The Visible Infrared Imaging Radiometer Suite (VIIRS) sensor onboard the Suomi National Polar Orbiting (S-NPP)  
32 satellite provides sets of aerosol environmental data records (EDRs) based on daily global observations from space

1 [Jackson et al., 2013; Liu et al., 2013]. Beginning in 2012, VIIRS provides AOT at 550 nm at a global 0.25 degree  
2 horizontal resolution. Daily gridded Enterprise Processing System (EPS) VIIRS data used are from the NOAA  
3 STAR ftp site at [ftp://ftp.star.nesdis.noaa.gov/pub/smcd/VIIRS\\_Aerosol/npp.viirs.aerosol.data/epsaot550/](ftp://ftp.star.nesdis.noaa.gov/pub/smcd/VIIRS_Aerosol/npp.viirs.aerosol.data/epsaot550/).

- 4 3) The Aerosol Robotic Network (AERONET), which is a global ground-based network of automated sun-photometer  
5 measurements, provides AOT, surface solar flux and other radiometric products [Holben et al., 1998]. It is a well-  
6 established network of over 700 stations globally and its data are widely used for aerosol-related studies [Zhao et al.,  
7 2002]. AERONET employs the CIMEL sun-sky spectral radiometer, which measures direct sun radiances at eight  
8 spectral channels centered at 340, 380, 440, 500, 675, 870, 940 and 1020 nm. AOT uncertainties in the direct sun  
9 measurements are within  $\pm 0.01$  for longer wavelengths (longer than 440 nm) and  $\pm 0.02$  for shorter wavelengths  
10 [Eck et al., 1999]. Table 1 lists number of stations, their location in terms of latitude and longitude. The stations are  
11 selected based on years in service and geographic location near the aerosol source regions. Stations covered major  
12 aerosol sources: African Dust, Southern Africa and South America (major forest fire stations), mixed aerosol  
13 regimes (urban areas in Europe, Asia and N. America), high latitude stations (capture major transport of forest fires  
14 from Siberia and Canada).
- 15 4) The Atmospheric Tomography Mission (ATom) studies the impact of human-produced air pollution on greenhouse  
16 gases and on chemically reactive gases in the atmosphere [Wofsy et al., 2018]. ATom deploys instrumentation to  
17 sample atmospheric composition, profiling the atmosphere in 0.2 to 12 km altitude range. Flights took place in each  
18 of 4 seasons over a 22-month period in 2016 through 2018. They originated from the Armstrong Flight Research  
19 Center in Palmdale, California, flew north to the western Arctic, south to the South Pacific, east to the Atlantic,  
20 north to Greenland, and returned to California across central North America over the Pacific and Atlantic oceans  
21 from  $\sim 80^\circ\text{N}$  to  $\sim 65^\circ\text{S}$ . In August 2016, PALMS was sampling on the NASA DC-8 aircraft as part of the ATom  
22 program (<https://espo.nasa.gov/missions/atom/content/ATom>). Aerosol composition determinations using the  
23 PALMS instrument during ATom-1 have been described and interpreted previously [Murphy et al., 2018, 2019;  
24 Schill et al., 2020; Bourgeois et al., 2020]. The PALMS mass concentrations for various species are derived by  
25 normalizing the fractions of particles of each size and type to size distributions measured by optical particle  
26 counters [Froyd et al., 2019].

### 27 2.2.3 Model ensemble analysis AOD and other model forecasts

- 28 1) International Centers for Aerosol Prediction - Multi-Model Ensemble (ICAP-MME) provides daily 6-hourly  
29 forecasts of total and dust AOD globally out to 120 h at 1 degree horizontal resolution [Reid et al., 2011; Sessions et  
30 al., 2015; Xian et al., 2019]. Total AOD in ICAP-MME is provided by the four core multispecies models: the  
31 European Centre Medium Range Weather Forecasts Copernicus Atmosphere Monitoring Service (ECMWF-  
32 CAMS), the Japan Meteorological Agency Model of Aerosol species in the Global Atmosphere (JMA-  
33 MASINGAR), the NASA Goddard Earth Observing System Version 5 (NASA-GEOS-5) and the Naval Research  
34 Lab Navy Aerosol Analysis and Prediction System (NRL-NAAPS) modeling systems. Dust-only AOD is provided

1 by the aforementioned four models, plus the Barcelona Supercomputer Center Chemical Transport Model  
2 (NMMB/BSC-CTM), the United Kingdom Met Office Unified Model (UKMO-UM) and NGACv2. However, the  
3 NGACv2 is only used for dust AOD in ICAP-MME, not use to compute ensemble mean in ICAP-MME for total  
4 AOD. All four of the multispecies models incorporate aerosol data assimilation (DA) and satellite-based smoke  
5 emissions. ICAP-MME is able to provide real-time comparison for synchronous evaluation of operational forecast.  
6 The correlation and RMSE between ICAP-MME and AERONET indicating in Table 1 shows that ICAP analysis is  
7 quite close to observation, which is good to use it as the global evaluated data, especially when the MERRA-2 data  
8 is not available in the real-time or operational forecast.

- 9 2) The NEMS GFS Aerosol Component Version 2.0 (NGACv2) for global multispecies aerosol forecast developed by  
10 NCEP and collaborators was previously used to provide operational global multispecies aerosol forecasts at NCEP  
11 [Wang et al., 2018]. The anthropogenic emissions are based on EDGAR V4.1 [Janssens-Maenhout, 2010] and  
12 AeroCom Phase II [Diehl et al., 2012]. The fire Emissions of carbonaceous aerosols and SO<sub>2</sub> are from Global  
13 Biomass Burning Emission Product-extended [GBBEPx, Zhang et al. 2014]. GBBEPx emissions are blended from  
14 NESDIS's Global Biomass Burning Emission Product from a constellation of geostationary satellites [GBBEP;  
15 Zhang et al., 2012] and GMAO's Quick Fire Emissions Data Version 2 from polar-orbiting satellites [QFED2;  
16 Darmenov and da Silva, 2015].
- 17 3) NGACv2 uses the same physics package as the 2015 version of the operational GFS.  
18 NGACv2 included additional aerosol species of sea salt, sulfate, organic carbon, and black carbon from the updated  
19 GOCART modules. Both science and software upgrades in the global forecast system were updated and  
20 implemented into NGACv2 in March 2017 to provide 5-day multispecies aerosols forecast products at the T126  
21 L64 resolution, approximately 100 km. The comparison of model configurations for GEFS-Aerosols and NGACv2  
22 has been shown in Table 2 based on the model information from Wang et al. [2018].

### 23 3. Emissions

#### 24 3.1. Anthropogenic emissions and background fields

25 The preprocessor PREP-CHEM-SRC v1.7, a comprehensive tool that prepares emission fields of trace gases and aerosols for  
26 use in atmospheric chemistry transport models, was used to generate the anthropogenic emissions, background fields of OH,  
27 H<sub>2</sub>O<sub>2</sub>, NO<sub>3</sub>, DMS and dust scheme input of clay and sand at the FV3 grid resolution for GEFS-Aerosols [Freitas et al., 2011].  
28 Two global anthropogenic emission inventories were chosen as input to drive the model, both providing monthly emissions.  
29 One is from the Community Emissions Data System (CEDS), which provides the emissions of BC, OC and SO<sub>2</sub> in 2014  
30 with 0.5 degree horizontal resolution [Hoesly et al., 2018]. The CEDS inventory improves upon existing inventories with a  
31 more consistent and reproducible methodology applied to all emission species, updated emission factors, and more recent  
32 estimates in 2014. The data system relies on existing energy consumption data sets and regional and country-specific

1 inventories to produce trends over recent decades [Hoesly et al., 2018]. The Hemispheric Transport of Air Pollution (HTAP)  
2 version 2 [Janssens-Maenhout et al., 2015] inventory provides the emissions of BC, OC, SO<sub>2</sub>, PM<sub>2.5</sub> and PM<sub>10</sub> in 2010.  
3 Figure 3 shows the comparisons of anthropogenic emissions between CEDS and HTAP for SO<sub>2</sub>, BC and OC in July. Aside  
4 from the shipping lanes showing up in CEDS, there is generally broader spatial coverage in CEDS. For SO<sub>2</sub>, the CEDS  
5 emissions are much larger over the eastern US, eastern China and Europe. Much higher values of BC and OC are seen in  
6 CEDS over Eastern Asia, South Asia and Europe. Similarly, much larger values for BC and OC are seen in the Southern  
7 Hemisphere in CEDS. We performed experiments by comparing model predictions using these two different anthropogenic  
8 emissions datasets with ATom-1 observations (figures not shown here). Slight improvements in SO<sub>2</sub> correlations and bias  
9 are seen and the sulfate, OC and BC biases improve over the Atlantic Ocean when using the CEDS emissions in comparison  
10 with the HTAP dataset. It should be noted that these anthropogenic emissions data are not impossible to catch up the date of  
11 real-time forecast. And it normally has time lag and represents the emissions of a different previous years. The inconsistency  
12 may have some impact on the predictions in 2019. But that is the most recently available version of anthropogenic emission.  
13 It is well known that strong actions have been taken to improve the worsening atmospheric environment and decrease the  
14 emission over China in the last 10 years [Chen et al., 2017; Zhang et al., 2012; Liu et al., 2016]. Considering the decreasing  
15 emission trend over China, the CEDS 2014 anthropogenic would result in some overprediction after 2014.  
16 We validated the GOCART background fields of OH and H<sub>2</sub>O<sub>2</sub> against the ATom-1 observations. Even though these  
17 background fields are model-derived climatologies, they both compare very well with the ATom-1 measurements. The  
18 newer NASA GEOS/GMI fields show improvement in the model-measurement biases for both OH and H<sub>2</sub>O<sub>2</sub>.

### 19 **3.2 Biomass burning emission**

20 The operation of GEFS-Aerosols is using the GBBEPx v3 emission with Fire Radiative Power (FRP). The GBBEPx v3  
21 system produces daily global biomass burning emissions of PM<sub>2.5</sub>, BC, CO, CO<sub>2</sub>, OC, and SO<sub>2</sub> by blending fire  
22 observations from MODIS Quick Fire Emission Dataset (QFED), VIIRS (NPP and JPSS-1) fire emissions, and Global  
23 Biomass Burning Emission Product from Geostationary satellites (GBBEP-Geo). GBBEP-Geo also produces hourly  
24 emissions from geostationary satellites, at individual fire pixels. In the results shown here, GBBEPx v3 daily biomass  
25 burning emissions on the FV3 C384 global grid are used for GEFS-Aerosols. The details of the GBBEPx v3 algorithm can  
26 be found in [https://www.ospo.noaa.gov/Products/land/gbbepx/docs/GBBEPx\\_ATBD.pdf](https://www.ospo.noaa.gov/Products/land/gbbepx/docs/GBBEPx_ATBD.pdf).

27 A one-dimension (1-D) time-dependent cloud module from High-Resolution Rapid Refresh (HRRR)-Smoke model has been  
28 implemented into GEFS-Aerosols to calculate injection heights and emission rates online [Freitas et al., 2007]. The new  
29 scheme in HRRR-Smoke is a modified version of the 1D plume rise scheme used in WRF-Chem [Freitas et al., 2007]. The  
30 new plume rise scheme is using the FRP data instead of the look-up table to estimate the fire heat fluxes [Ahmadov et al.,  
31 2017]. The 1-D cloud module is able to be applied GBBEPx v3 fire emissions datasets to account for plume-rise that  
32 distributes the fire emissions vertically and better simulate the fire events and pollution transport of smoke plumes.

1 To validate model performance when using the GBBEPx v3 fire emissions with a plume-rise module based on real-time FRP  
2 data, we compare the real-time GEFS-Aerosols AOD with other reanalysis data, satellite observations and the NGACv2  
3 model for the big fire event in August 2019. Smoke from large fires burning in the Amazon rainforest, primarily in Brazil,  
4 Bolivia, Paraguay, and Peru, stretched over northern South America in mid-August. Figure 4 shows the total AOD forecast  
5 on 25th August compared against the NGACv2 model, MERRA-2 reanalysis data and satellite observations of VIIRS and  
6 MODIS. For both satellites, daily gridded AOD is used to compare against the model forecast at 18z. The GEFS-Aerosols  
7 AOD is able to reproduce the enhanced AOD due to several fire events over South America near the border of Bolivia,  
8 Paraguay, and Brazil, which were also observed by the VIIRS and MODIS satellite instruments and captured by the  
9 MERRA2 analysis. Although there are a lot of missing data downwind from the fires in the satellite observations of VIIRS  
10 and MODIS, especially over the south Pacific, GEFS-Aerosols and MERRA-2 results are consistent in showing the transport  
11 of fire plumes into the tropical Pacific and southern Atlantic. In contrast, the NGACv2 model does not capture these fire  
12 events, and exhibits only a very slight AOD enhancement. NGACv2 AOD is more than 80% smaller than the observations  
13 over the fire source region and produces little or no transported smoke over the surrounding areas.

14 Beyond the fires burning in South America, an even greater number of blazes on the African continent are observed by the  
15 satellite images at almost the same time in August 2019. Angola experienced almost three times more fires than Brazil in the  
16 middle of August 2019. There were around 6,000 fires in Angola, more than 3,000 in Congo and just over 2,000 in Brazil,  
17 according to NASA satellite imagery (<https://earthobservatory.nasa.gov/images/145421/building-a-long-term-record-of-fire>).  
18 One of the main large-scale aerosol features of Sub-Saharan Africa is the June-to-September biomass burning season in  
19 Angola, Congo, and Zambia [Bauer et al., 2019]. Overall, the GEFS-Aerosols model reasonably simulates the major burning  
20 event on August 25<sup>th</sup>, 2019 over southern Africa (Figure 4), but overestimates the central African plume when compared  
21 with the MERRA2 analysis. The satellite AOD retrievals of VIIRS and MODIS off the coast of central Africa are  
22 challenging due to screening by the stable stratiform cloud deck over the ocean that occurs during the fire season, creating  
23 less reliable coverage from these observational data. Nevertheless, we can still see consistent AOD enhancements over the  
24 fire source regions and surrounding areas for both GEFS-Aerosols and the observations. NGACv2, however, is quite  
25 different from the satellite observations and MERRA2 analysis, underestimating the AOD more than 50-90% percent over  
26 the southern Africa fire source region and showing little obvious enhancement. Obviously, the updates in fire emission using  
27 GBBEPx v3 emission and FRP by applying the 1D plume rise scheme in GEFS-Aerosols model show great improvements in  
28 the AOD forecast during the fire events compared to the NGACv2 (Table 2).

29 Future work will explore the use of diurnal fire profiles based on historic GOES fires products applied to estimate biomass  
30 burning emissions to enhance forecast behavior. Additionally, a parameterization based on fire weather index (FWI) to  
31 estimate biomass burning emissions on longer temporal scales may help to improve and extend the forecast of fire impacts.

#### 32 **4. Real-time forecast Evaluation**

## 1 4.1 Evaluation of global AOD

2 A real-time forecast was performed starting on July 1 2019 on ~25km resolution and continuing to the present day using the  
3 GBBEPx v3 fire emissions with the plume-rise module based on real-time FRP data.

4 We evaluated the GEFS-Aerosols model performance with the daily AERONET data globally. The locations of the 60  
5 selected AERONET sites where these comparisons were made are listed in Table 1. It also indicates the correlation and  
6 RMSE of GEFS-Aerosols, ICAP and NGACv2 AOD with respect to that of AERONET observation. The GEFS-Aerosols,  
7 NGACv2 and ICAP predictions are sampled at the same locations as the AERONET sites for these comparisons. The left  
8 panel in Figure 5 (a and b) shows the correlation coefficients between daily total AOD observed by AERONET and the day  
9 1 forecast of model AOD from GEFS-Aerosols and NGACv2 for the period between 7/5/2019 and 11/30/19. The correlation  
10 coefficients range from 0.5 to 0.9 for GEFS-Aerosols at most sites, except for several sites in South America, Africa and  
11 eastern Asia near fire source regions, which are slightly lower than those of the ICAP. In contrast, the correlation  
12 coefficients of daily total AOD between the NGACv2 and AERONET observations are lower than 0.5 globally, even  
13 ranging from 0.1 to 0.3 at most sites. A more quantitative display of correlation coefficients for a selection of 60 AERONET  
14 sites for GEFS-Aerosols and NGACv2 is presented in Table 1. This comparison strongly indicates the improved  
15 performance of total AOD daily variation in GEFS-Aerosols prediction when compared with NGACv2. There are 20 sites  
16 (about 30% of total sites) displaying highly correlated total AOD for the AERONET data and GEFS-Aerosols, with the  
17 correlation coefficients exceeding 0.7. In contrast, there is only 1 site with a correlation coefficient larger than 0.7 for  
18 NGACv2 model vs. AERONET, and 19 sites have correlation coefficients that are less than 0.2 for AERONET and  
19 NGACv2. Fig. 5 c and are the RMSE of GEFS-Aerosols and NGACv2 with respect to AERONET observation. Most of  
20 RMSE values are below 0.25 in GEFS-Aerosols over North America, Europe and Africa. However, the RMSE values in a  
21 lot of sites over Africa and Asia are above 0.3 in NGACv2. From Table 1, the ICAP results show the best performance in  
22 both the correlation and RMSE.

23 In addition to comparing with the AERONET data, Fig. 6 shows the Day 1 AOD prediction of GEFS-Aerosols and NGACv2  
24 compared with the MERRA-2 reanalysis and MODIS observations averaged from July to November 2019. The GEFS-  
25 Aerosols prediction is able to capture the geographical features of AOD as represented by the MERRA-2 reanalysis data and  
26 MODIS satellite observations, such as the dust plumes over North Africa and the Arabian Peninsula, biomass burning  
27 plumes in southern Africa, south America, northwestern America and eastern Europe, polluted air over eastern and southern  
28 Asia, and high-latitude sea-salt bands over the southern hemisphere. The high AOD over southern Africa and northern India  
29 is more comparable to the MODIS observation than that of NGACv2. As pointed out by Bhattacharjee et al. [2018], the NGACv2  
30 predictions exhibit widespread underestimates over most of these high AOD regions, such as eastern Asia, and fire source  
31 regions of southern Africa, eastern Europe, southeastern Asia.

32 Figure 7 indicates the Day 1 AOD forecast biases of GEFS-Aerosols and NGACv2 with respect to MERRA-2 reanalysis  
33 between 7/5/2019 and 11/30/19 for dust, OC and sulfate. The predicted dust AOD in GEFS-Aerosols is quite comparable to

1 that of MERRA-2 results, with only small negative biases of  $\sim 0.08$  over Asia and the downwind areas of African dust source  
2 regions of Atlantic and south Asia (Figure 8a). GEFS-Aerosols has some small positive biases relative to MERRA-2 of  $\sim 0.1$   
3 over Australia (in red). In contrast, dust AOD in NGACv2 (Figure 8b) shows large over predictions of MERRA-2 over  
4 Africa with maximum value  $\sim 0.45$  and about 0.02-0.05 over large areas of Asia and North Pacific and North America.  
5 Wang et al. [2018] also showed that the predicted dust AOD in NGACv2 over northwestern Africa is much larger than  
6 GEFS-Aerosols, MERRA-2 and MODIS observations.

7 OC is a major component emitted from wildfires, and OC AOD is a good indicator of the performance of fire impacts.  
8 GEFS-Aerosols OC AOD shows smaller biases compared to the MERRA-2 reanalysis than those of NGACv2 (Figure 7c  
9 and d). Positive biases in GEFS-Aerosols OC AOD of less than 0.2 occur mainly over southern Africa, eastern Asia, south  
10 Asia and the Middle East. The GEFS-Aerosols overprediction of OC AOD compared with MERRA-2 over eastern China  
11 may be associated with the overestimate of anthropogenic emissions by using CEDS 2014, since this is not a major fire  
12 source region. GEFS-Aerosols shows small negative biases, of less than 0.1, over South America and middle and eastern  
13 Europe. Overall, the biases of OC AOD in NGACv2 relative to MERRA-2 are dominated by under prediction globally with  
14 the largest biases of more than 0.3 over major fire source regions of southern Africa, the Amazon region of South America,  
15 Southeastern Asia and Siberia (Figure 7d).

16 For sulfate AOD, the GEFS-Aerosols forecast over predicts MERRA-2 by  $\sim 0.08$  over eastern Africa, the Middle East, and  
17 southeastern China, where  $\text{SO}_2$  anthropogenic emissions are dominant. Small GEFS-Aerosols under predictions, less than  
18 0.1 AOD, are seen over broad areas of the Northern Hemisphere, such as eastern North America and its downwind areas  
19 over the north Atlantic and western Europe, as well as eastern Asia and its downwind areas (Figure 7e). As in the case of OC  
20 AOD, the global sulfate AOD in MERRA-2 is under predicted significantly by NGACv2 (Figure 7f). The areas with the  
21 largest NGACv2 vs. MERRA-2 sulfate bias are mainly over the major anthropogenic source regions, such as India and  
22 eastern China, where the underestimates exceed 0.18, and in the eastern US and western Europe, where they exceed 0.1.

23 The summary comparison of the GEFS-Aerosols and NGACv2 Day 1 total AOD prediction biases with respect to MERRA-  
24 2 reanalysis between 7/5/19 and 11/30/19 is shown in Figure 8. Generally, the GEFS-Aerosols model is able to reproduce the  
25 total AOD very well, much better than NGACv2 (see Figure 8a and b). The GEFS-Aerosols over predictions over eastern  
26 China and Southern Hemisphere ( $\sim 0.2$ - $0.3$ ) are mainly due to anthropogenic OC and  $\text{SO}_2$  for the former and fire emissions  
27 of OC for the latter, respectively. Both GEFS-Aerosols and NGACv2 total AOD have small negative biases ( $\sim 0.3$ - $0.5$ )  
28 relative to MERRA-2 over the northwestern China dust source region. Negative biases of GEFS-Aerosols vs. MERRA-2 in  
29 South America may be caused by inadequate fire emissions and in Europe that may be related to anthropogenic  $\text{SO}_2$   
30 emissions. The spatial locations of biases in GEFS-Aerosols with respect to MERRA-2 reanalysis total AOD (Figure 8a) are  
31 similar to the comparisons with the individual aerosol species from MERRA-2 discussed above (Figure 7a, c and e). The  
32 NGACv2 total AOD is biased low relative to MERRA-2 almost globally except for the over prediction over North Africa  
33 due to dust (Figure 8b). The largest NGACv2 total AOD biases are mainly caused by the under predictions of fires over the  
34 fire source regions of South America, southern Africa, Southeastern Asia and middle and eastern Europe and the

1 anthropogenic source regions over eastern China, India and eastern North America, with maximum total AOD biases  
2 reaching more than 0.5.

### 3 **4.2 Evaluation of AOD associated with fire events**

4 We choose some sites near the major fire source region, which have available observation data for the duration of this study  
5 and hold long records based on various previous studies. Figure 9 indicates the total AOD time series of AERONET  
6 observations compared against ICAP, NGACv2 and GEFS-Aerosols model predictions at the four AERONET sites near the  
7 fire source regions of South America during the period of 7/1/19-11/30/19. At the Alta Floresta site, which is in the middle  
8 of Amazon fire source region, the daily AOD variations of both the ICAP and GEFS-Aerosols day 1 predictions are quite  
9 consistent with that of the AERONET data, especially as they are able to reproduce two peaks in AOD enhancements in late  
10 August and late September caused by fire plumes (Figure 9a). The correlation (RMSE) is 0.66 (0.23), 0.9 (0.12) and 0.68  
11 (0.31) for GEFS-Aerosols, ICAP and NGACv2. Obviously, NGACv2 results under predict AERONET observations almost  
12 throughout the whole period with a significantly larger bias than GEFS-Aerosols or ICAP, and the two August-September  
13 peaks in total AOD enhancements are essentially missed in the NGACv2 prediction.

14 The Itajuba site is located southeast of the Alta Floresta site and in the downwind areas of the Amazon fire source region.  
15 The total AOD time series of GEFS-Aerosols prediction matches closely those of ICAP and AERONET during most of the  
16 time period, though there are some discrepancies from the end of August to middle September when the GEFS-Aerosols  
17 underpredicts the high AOD episode (Figure 9b). GEFS-Aerosols is able to predict the two AOD enhancements in mid-  
18 October and early November, which is quite comparable as ICAP. The correlation (RMSE) is 0.856 (0.15) and 0.936 (0.09)  
19 for GEFS-Aerosols and ICAP with respect to AERONET at the site of Itajuba, only 0.451 (0.22) for NGACv2. The  
20 NGACv2 prediction also generally underestimates the observations at this site too (Figure 9b). The NGACv2 results are  
21 closer to the ICAP, GEFS-Aerosols and AERONET before August, and NGACv2 shows a slight increase of total AOD in  
22 early September, but the NGACv2 AOD magnitude is much lower than the AERONET by about a factor of 5-7 from the  
23 middle of August onward.

24 Located in the southern part of the Amazon fire region, the site of Santa Cruz Utepsa is south of the AltaFloresta site. The  
25 correlation (RMSE) values of GEFS-Aerosols and ICAP with respect to AERONET are 0.8 (0.18) and 0.88 (0.13)  
26 respectively, which shows better performance than those of NGACv2 with 0.3 (0.39) at this site in predicting the total AOD  
27 through the 5 months from July to November (Figure 9c). The model not only reproduces the total AOD temporal variation  
28 of the AERONET results, but also captures several fluctuations of high AOD in August and September caused by Amazon  
29 fire events. Again, some of fluctuations in total AOD were captured by the NGACv2 prediction, but the modeled AOD  
30 magnitudes are 2-4 times lower than the observations.

31 The last site of RioBranco is also located in the Amazon fire source region but to the west of the AltaFloresta site. There are  
32 some missing data at this site for the AERONET total AOD from middle July to middle September (Figure 9d). During this



1 period, the GEFS-Aerosols prediction is slightly lower than ICAP by about 5-10%. Both ICAP and GEFS-Aerosols total  
2 AOD match the AERONET variations well when the AERONET data are available again from mid-September. Several  
3 peaks of total AOD are also captured by GEFS-Aerosols in middle September and early November. The NGACv2 prediction  
4 shows enhanced total AOD in middle August, with low biases by more than 2-3 times compared to ICAP and GEFS-  
5 Aerosols. For other enhancements of total AOD after October, the NGACv2 results completely miss the fire events and do  
6 not show any fluctuations. The correlation (RMSE) is 0.80 (0.24) and 0.90 (0.17) for GEFS-Aerosols and ICAP with respect  
7 to AERONET at the site of RioBranco, only 0.51 (0.44) for NGACv2.

8 We also evaluate the total AOD time series of AERONET against ICAP, NGACv2 and GEFS-Aerosols for fire regions of  
9 central and southern Africa. The comparisons at seven AERONET sites from July to November are shown in Figure  
10 10. Generally, the GEFS-Aerosols predictions are able to capture the daily total AOD variation measured by AERONET. At  
11 the site of Misampfu, the GEFS-Aerosols mode is somewhat better than that of ICAP in predicted the peaks of high AOD.  
12 The correlation coefficients at the sites of Ascension Island and Lubango are much high than those of ICAP (see Table 1).  
13 While both the GEFS-Aerosols and ICAP overpredicted the total AOD most of time throughout the three months at the  
14 station Bamenda located north of the major African fire source region. The NGACv2 total AOD forecast shows under  
15 prediction at most of the AERONET sites in this region. Meanwhile, NGACv2 and ICAP predictions are not consistent with  
16 AERONET either, especially for several observed high peaks which are not reproduced by the model results (e.g. Gabon).  
17 At the remote site of Ascension Island located west of the African fire source region, the GEFS-Aerosols and ICAP are able  
18 to capture the AOD enhancements in the middle of August, and shows the best performance of the three different models  
19 (see Table 1). For other sites that are located in the fire source region, such as Monguinn, Misampfu, Maun Tower, and  
20 Lubango, the prediction of the GEFS-Aerosols model shows higher correlation of 0.68, 0.79, 0.84 and 0.71 than those of  
21 NGACv2 as 0.51, 0.26, 0.29, 0.35. The RMSE values of GEFS-Aerosols are 0.18, 0.15, 0.10, 0.15, which is much lower  
22 than the NGACv2 of 0.32, 0.34, 0.23, and 0.32. It suggests that the GEFS-Aerosols better matches the observed temporal  
23 variation of total AOD than NGACv2. One peak in early August at the Monguinn site, one peak in middle September at the  
24 Misampfu site, two peaks in early August and early September at Maun Tower site and one enhancement in August at  
25 Lubango are all predicted by the GEFS-Aerosols model. The ICAP forecasts shows lower biases against the AERONET  
26 total AOD for predicting these peaks, while none of these peaks are captured by NGACv2. GEFS-Aerosols shows slight  
27 over predictions in mid-July and late August for Gabon and early August for Lubango.

#### 28 **4.3 Evaluation of AOD associated with dust events**

29 Thirteen AERONET sites inside the major dust source regions of western North Africa, Asia and the Middle East and  
30 surrounding areas have available data from July to November 2019. The total AOD time series of GEFS-Aerosols, ICAP,  
31 and NGACv2 at 6 of these sites are shown in Figure 11. Overall, the GEFS-Aerosols model is able to closely predict the  
32 observed total AOD variation, especially at the sites of Banizoumbu, Tenerife, Saada, Ben Salem, Granada and Sede Boker,

1 with much better performance than those of NGACv2 according to the correlation (RMSE) values in Table 1 of GEFS-  
2 Aerosols as 0.74 (0.15), 0.77 (0.07), 0.76 (0.14), 0.82 (0.07), 0.85 (0.09), and 0.73 (0.08) versus NGACv2 as 0.33 (0.24),  
3 0.25 (0.18), 0.25 (0.26), 0.25 (0.23), 0.21 (0.16), and 0.19 (0.14) . In addition to NGACv2's overprediction at the sites of  
4 Ben Salem and Granada, it does not accurately capture observed temporal variations of total AOD at these sites.  
5 We compare the daily AERONET total AOD with the 1-day forecasts of total AOD from GEFS-Aerosols and NGACv2 at  
6 the AERONET sites of Cape Verde, Tamanrasset and Tenerife located in the dust source region over North Africa in Figure  
7 12. The slope of the linear regression of AERONET total AOD vs. GEFS-Aerosols is quite different from that of NGACv2  
8 at the site of Tamanrasset, which is located in southern Algeria and in the middle of the Saharan dust source region. The  
9 GEFS-Aerosols linear regression slope is much closer to 1 than that of NGACv2, and the  $R^2$  in the NGACv2 model is lower  
10 by a factor of 4 than that of the GEFS-Aerosols model at this site. At the other two sites of Cape Verde and Tenerife, which  
11 are in the downwind area west of the African dust source region, the slopes of the linear regressions for GEFS-Aerosols are  
12 also much closer to 1 than those of the NGACv2 model. The NGACv2 model, as evidenced by the  $R^2$  values, is more poorly  
13 correlated with AERONET than the GEFS-Aerosols prediction. The  $R^2$  values of GEFS-Aerosols is 0.50, 0.33 and 0.59 in  
14 these sites, which better captures the dust transport in the downwind areas west of the African dust source region than the  
15 NGACv2 model as 0.19, 0.08 and 0.06. GEFS-Aerosols model is using FENGSH dust scheme, which is quite different to the  
16 GOCART dust scheme using in NGACv2, which shows significant improvements in the dust AOD predictions.

#### 17 **4.4 Evaluation of major regional averages**

18 Figure 13 shows day 1 predictions of total AOD time series by GEFS-Aerosols and NGACv2 compared against the  
19 MERRA-2 reanalysis averaged over 9 major global regions from August 2019 to March 2020. The comparison clearly  
20 shows the consistency between GEFS-Aerosols and the MERRA-2 reanalysis over most of these 9 regions, especially North  
21 Africa, the North Atlantic, Southern Africa, and the South Atlantic, with only minor discrepancies during these 8  
22 months. The total AOD is dominated by dust in North Africa and fire emissions in Southern Africa. The aerosols emitted  
23 from dust and fire regions and their long-range transport play important roles in impacting the total AOD over the North and  
24 South Atlantic Oceans. The good agreement with MERRA-2 shows that GEFS-Aerosols captures the emissions and  
25 transport of dust and fire emissions in these regions.

26 Total AOD variation in South America is mainly related to biomass burning emissions. GEFS-Aerosols has some slight low  
27 biases relative to MERRA-2 from middle September to early October 2019 that are associated with the Amazon fire event.  
28 GEFS-Aerosols under predicts MERRA-2 in this region from mid-November 2019 to March 2020, outside the main biomass  
29 burning season, which suggests that the GEFS-Aerosol AOD low biases in this region are mostly associated with sources  
30 other than fires.

31 The European region has the largest differences between GEFS-Aerosols and MERRA-2 reanalysis total AOD among the 9  
32 regions. Although their temporal variations are similar, GEFS-Aerosols under predicts the MERRA-2 total AOD throughout

1 the whole period by a factor of 0.5. The large absolute low biases from August to early October 2019 and March 2020 in  
2 Europe which are associated with GEFS-Aerosols underestimates of sulfate AOD (Fig. 8).  
3 From August to early December 2019, the GEFS-Aerosols total AOD looks quite consistent with the MERRA-2 reanalysis  
4 on average across East Asia. GEFS-Aerosols high biases starting in middle December 2019 and increasing from January to  
5 March 2020 may be associated with the lockdown in China during the Coronavirus disease 2019 (COVID-19) pandemic.  
6 Anthropogenic emissions of NO<sub>2</sub>, SO<sub>2</sub>, VOC, and primary PM<sub>2.5</sub> over the North China Plain during this period were reduced  
7 by 51%, 28%, 67% and 63%, respectively, compared to the previous year, resulting in lower surface aerosol and ozone  
8 levels and improvements to air quality [Shi and Brasseur, 2020; Wang and Su, 2020; Xing et al., 2020]. Since the  
9 anthropogenic emissions used in GEFS-Aerosols are based on the CEDS 2014 inventory, they definitely overestimate the  
10 anthropogenic aerosol emissions during the 2019-2020 lockdown periods.

11 Both the Eastern and Western US regions exhibit GEFS-Aerosols low biases of about 5-30%, with the largest differences in  
12 Eastern US occurring in August 2019. However, the trends of total AOD temporal variations with low in summer and high  
13 in winter in the GEFS-Aerosols prediction and the MERRA-2 reanalysis are quite consistent over Eastern and Western US.  
14 The minor under predictions by GEFS-Aerosols need further investigation.

15 In comparison, the NGACv2 predictions show significant under prediction of MERRA-2 total AOD for almost all of these 9  
16 regions throughout this 8-month period. The one exception is North Africa, where the NGACv2 results are close to the  
17 MERRA-2 reanalysis, with over prediction in August 2019 and low biases from December 2019 to March 2020. In addition  
18 to its general under prediction of MERRA-2 total AOD, NGACv2 is not able to capture the temporal variations of total AOD  
19 in some regions, such as the enhanced AOD due to fire emissions in Southern Africa, South Atlantic and South America.  
20 Though NGACv2 shows similar temporal variations to MERRA-2 total AOD in Europe, East Asia, and the US, the  
21 magnitudes of NGACv2 predictions are too low by a factor of 1 to 3. This analysis is consistent with a 1-year evaluation of  
22 GEFS-Aerosols AOD that shows improvements over NGACv2 [Bhattacharjee et al., 2021]

## 23 **5. ATom-1 retrospective forecast evaluation**

24 Retrospective simulations of GEFS-Aerosols and NGACv2 were performed for the summer of 2016 and evaluated using  
25 aircraft measurements from the first deployment of the Atmospheric Tomography Mission (ATom-1) in July and August  
26 2021. During ATom-1, plumes from dust storms and large biomass burning events and low-level sea salt aerosols were  
27 observed over the southern and central Atlantic, and anthropogenic pollution was observed over the United States on the last  
28 flight from Minnesota to Southern California.

29 In this section, we evaluate the 24-hour forecast skill of GEFS-Aerosols and NGACv2 by comparing with ATom-1  
30 observations. The GEFS-Aerosols and NGACv2 model results are sampled at the same latitude, longitude and altitude as the  
31 ATom-1 measurements. The model output is hourly with ~25km horizontal resolution on the FV3 native grid. The ATom-1  
32 measurements collected on a 1-second time base were compared to the nearest hour's model forecast. Model data is

1 interpolated vertically (according to log-Z above ground level), but sampled within the nearest horizontal grid as the  
2 observations (with no horizontal interpolation). Thus, the inherent differences between temporal (differences of up to 0.5  
3 hour) and spatial scales of the observations (~200 m resolution) and model results (25-100 km resolution) must be kept in  
4 mind with the model-measurement comparisons.

## 5 **5.1 Global flight track column sum comparisons**

6 Figure 14 shows the tropospheric column sums of OC along the flight tracks of the NASA DC-8 for the ATom-1  
7 observations and GEFS-Aerosols model experiments. The OC column sums using GBBEPx v3 fire emissions at ~25 km  
8 resolution (Fig. 14 (b)) are quite consistent and comparable to the observations. The modeled OC column sums are somewhat  
9 smaller than those of observation over the north Atlantic, Greenland, and southeastern Canada.

10 Results of the model-measurement comparisons for dust are shown in Figure 15. GEFS-Aerosols simulations show good  
11 agreement with ATom-1 observations over tropical north Atlantic and downwind of the western Africa dust source region.  
12 However, the model underestimates the dust columns over tropical south Atlantic, Greenland, southeastern Canada, while  
13 underestimating dust over the US, Alaska and broad areas of the Pacific Ocean. The GEFS-Aerosols model shows a clear  
14 enhancement of the dust event sampled on 8/17/16 east of the African coastline near 22°N, though the model column  
15 maxima tend to be more than a factor of 5 lower than the observations.

16 Table 3 gives median bias and correlation statistics for column sums of all GEFS-Aerosols model cases as well as the  
17 NGACv2 dust forecasts for ~130 profiles illustrated in Figures 14 and 15. Correlations ( $r$  – Pearson correlation coefficients)  
18 are typically above 0.7 for all species except dust. The OC differences noted above for GBBEPx v3 are apparent in the bias  
19 statistics of OC (a factor of 2.5) and BC (a factor of 50%), although R-correlations are not significantly affected. Differences  
20 in the fire inventories also affect sulfate biases slightly (12%). For all species except for dust, decreases in median  
21 model/observed ratios are seen for the model results.

22 Dust, on the other hand, shows a slight underprediction in column amount in the model results. Dust sources depend  
23 critically on surface wind speed, have very little overlap with the anthropogenic and biomass-burning sources of the other  
24 species, and are associated with areas of weather and surface conditions, all which may contribute to the different response  
25 of dust emissions. Correlations of dust are also much lower than for other species, and there is a very obvious difference  
26 between GEFS-Aerosols and NGACv2 model forecast statistics as discussed further below. We note that sea-salt columns  
27 are not calculated or compared to ATom-1 observations, due to the large amount of observations below the detection limit,  
28 especially above 2 km altitude.

## 29 **5.2 Vertical profile statistics comparisons**

30 ATom-1 flight tracks are separated into 2 sections and labeled as the “Pacific” side for July 29 to August 8 2016 flights and  
31 the “Atlantic” side for August 15 to August 23 2016 flights. For this analysis the 1-second model and observed data are

1 binned into 10 equally spaced vertical intervals (~1km) covering the vertical extent of the ATom-1 profiles. Figure 16 shows  
2 median, ratio and correlation statistics of OC, BC and sulfate for the 2 geographic regions and the two model cases. For OC  
3 over the Pacific, the median values are lower than that of the observation by more than 50%. Their correlations with  
4 observation are quite similar above ~3 km height. The vertical profile of ratio also suggests that the OC concentrations are  
5 underpredicted over Pacific. Statistics for the Atlantic flight tracks of ATom-1 show similar trends and behavior. The median  
6 values of model prediction OC are quite comparable to observations, which show very consistent vertical variation similar to  
7 the observations. The correlations with observations improve below 4 km height compared to those of the Pacific with the  
8 maximum closed to 0.80. While the correlations decrease significantly at 3-6 km height, it increases almost 50% above 6km  
9 height. The model results are biased too low below ~3km. The BC vertical profile statistics are quite different to OC with the  
10 model forecasts much larger than observations as one goes higher in altitude over both the Pacific and Atlantic section.  
11 Correlation coefficients with observations are about 0.6-0.8 from near surface to ~6km over Pacific and about 0.7-0.9 below  
12 ~4km over Atlantic. The correlations of both OC and BC decrease significantly above ~4km over the Atlantic. For sulfate,  
13 the median biases of model are biased too low from near surface to ~8 km over the Pacific and their correlation coefficients  
14 with observations are about 0.4-0.6 below 6 km. For the Atlantic, median values are quite comparable to the observation  
15 below ~7 km and their correlations are about 0.3~0.9 and consistently decreasing with altitude. By contrast, the Pacific  
16 comparisons for sulfate show a significant underprediction (60-70%) from the 0.5 to 7.0 km altitude for both model cases,  
17 which suggests a significant underprediction of oceanic gas-phase sulfur sources, such as DMS.  
18 Vertically resolved statistics of naturally occurring dust and sea salt are shown in Figure 17. For dust over the Pacific,  
19 median values of GEFS-Aerosols are too low while the NGACv2 results are too high compared with the observations, and  
20 the correlations are almost less than 0.5. The performance of GEFS-Aerosols improves over the Atlantic with median values  
21 comparable to observations above ~4km and the correlation coefficients increasing to 0.5~0.8 below ~5km. While it is still  
22 showing a significant high bias for the NGACv2 model over Atlantic. For sea salt, the median values biases are all biased  
23 too low over both the Pacific and Atlantic. Generally, the correlations are much better below ~6 km.

### 24 **5.3 Height-latitude profile comparisons over the Atlantic during ATom-1**

25 The ATom-1 flight profiles allow a more detailed comparison of aerosol spatial patterns from different aerosol sources with  
26 the model. High values of OC and BC from fires were observed on 8/15/16 and 8/17/16 over the Atlantic, as were high  
27 values of dust and sea-salt. The flight track of height-latitude profiles of OC, BC and sulfate for these combined days are  
28 shown in Figure 18 for the ATom-1 measurements and the model results. The model results show similar pattern as the  
29 ATOM-1 in reproducing the profiles of OC even using log scale, especially the biomass burning plumes near the tropics,  
30 though the model results show slightly low biases. But they also show some bias for OC at levels above 4~5 km over the  
31 north Atlantic, where model results show high biases. Overall, predicted BC (middle column of Figure 18) is able to capture  
32 the decreasing trend with increasing altitude in the latitude-height profiles, however they are underpredicted in the biomass

1 burning plumes near the tropics from the surface to 5 km height in both model experiments, which have been seen in other  
2 models due to insufficient wet scavenging [Wang et al., 2014, Choi et al., 2020]. Similar to the OC profiles, the model  
3 results overpredict above 4-5 km height levels. It appears the model does not reproduce the enhancements of BC at 1-4 km  
4 height very well over this area. It may be possibly due to relative weak convection or a low modeled injection height that the  
5 fire emission has not been lifted enough to this altitude, which need further studies. For sulfate (right column), the model  
6 experiments show high concentrations at low altitude, similar to the observations, though there are still some differences for  
7 the plume location at 2-4 km height that shift the plume from near the equator to near 20°N in the model experiments. Over  
8 the equatorial areas at about 2-4 km height, the observed sulfate concentration is underestimated by about 30% by modeled  
9 results, which may also relate to the injection height of biomass burning those results in much lower SO<sub>2</sub> at this altitude since  
10 SO<sub>2</sub> is one of the important precursors for sulfate production. Meanwhile, the sulfate concentration above 6 km is  
11 overestimated over the tropics while underestimated near the surface.

12 Figure 19 shows the comparisons of the naturally occurring dust and sea salt aerosols for the same time period. In the left  
13 column of dust, we also include the NGACv2 results. For more consistent comparisons, here the modeled dust results are  
14 summed up by the first two bins to match the observation particle size range (less than 3 μm). The GEFS-Aerosol  
15 predictions show agreement in the dust height-latitude profiles with the observations and exhibit similar patterns. The  
16 observed dust plumes are reproduced by the model over 15-35°N, but the model appears to underestimate wet removal in the  
17 upper levels that results in the overestimation of dust above 7-8 km height in northern Atlantic and above 5 km height in the  
18 tropical southern Atlantic. On the other hand, the NGACv2 prediction shows a very large bias over broad areas of the north  
19 Atlantic and the tropical southern Atlantic. A high dust plume near 35°S has not been captured well by the model from the  
20 surface to the upper levels, which may be caused by missing dust events over South America. For sea salt, the model results  
21 are able to predict patterns consistent with the observation, especially from the surface to about 4-6 km height.

## 22 **6. Summary and future plan**

23 Since the dynamical core of FV3 developed by GFDL has been selected by NOAA to be the dynamical core for the Next  
24 Generation Global Prediction System (NGGPS), development of a coupled weather and atmospheric chemical composition  
25 model for chemical weather and air quality forecasting based on the FV3 framework has begun couple of years ago. The  
26 development as a single ensemble member of the Global Ensemble Forecast System (GEFS) has been completed. This new  
27 model, referred to as GEFS-Aerosols, was implemented as one member of the GEFS into operations as part of NOAA's first  
28 coupled UFS model in September 2020 and replaced previous operational global aerosol prediction system NGACv2 at  
29 NCEP.

30 The chemical component of atmospheric composition in GEFS-Aerosols is based on WRF-Chem, which is a community  
31 modeling system used by thousands of users worldwide. The aerosol modules are based on modules from the GOCART  
32 model. Features of the new model include: 1) the biomass burning plume rise module added from WRF-Chem; 2) the

1 FENGSHA dust scheme implemented and developed by NOAA Air Resources Laboratory (ARL); 3) all sub-grid scale  
2 tracer transport and deposition is handled inside the physics routines requiring consistent implementation of positive definite  
3 tracer transport and wet scavenging in the SAS scheme; 4) the updated background fields of OH, H<sub>2</sub>O<sub>2</sub> and NO<sub>3</sub> from GMI  
4 model; 5) biomass-burning emission calculations based on the GBBEPx v3 emission and FRP provided by NESDIS; and 6)  
5 global anthropogenic emission inventories derived from CEDS and HTAP. These fundamental updates in GEFS-Aerosols  
6 indicate quite different features compared to the NGACv2 (see Table 2), including dynamical core, physics package,  
7 coupling infrastructure, horizontal resolution, and emission. These may play important roles in affecting the aerosol transport,  
8 wet and dry deposition, and emission etc., which would help to improve the model performance. This new model is able to  
9 forecast the higher-resolution distribution of primary air pollutants of aerosols: black carbon, organic carbon, sulfate, and  
10 dust and sea salt each with five size bins. Meanwhile, it is also capable of handling volcanic eruptions, which can inject vast  
11 quantities of particulates into the atmosphere. While for the predicted results in the paper, we have not included the volcanic  
12 emission into the model for the June 2019 Raikoke eruption, it may partially impact on the underprediction over high  
13 northern latitude.

14 The updates in anthropogenic and fire emission indicate that the GEFS-Aerosols shows much better performance matching  
15 the AOD observations when configured to use the CEDS anthropogenic emission and GBBEPx v3 fire emissions with  
16 plume-rise module compared to NGACv2, especially over the fire source regions. For more extensive evaluation, we  
17 performed 9 months of Day-1 real-time forecast of GEFS-Aerosols starting in July 2019 and the predicted AOD was used to  
18 compare with the satellite observations from MODIS and VIIRS, reanalysis data of ICAP-MME and MERRA-2, AERONET  
19 observations, and the model predictions from MERRA-2 and NGACv2. Overall, GEFS-Aerosols indicates substantial  
20 improvement for both composition and variability of aerosol distributions over those from the currently operational global  
21 aerosol prediction system of NGACv2. Globally, the GEFS-Aerosols predicted biases with respect to MERRA-2 forecast for  
22 dust, OC and sulfate AOD were improved compared to those from NGACv2. Substantial improvements were seen for the  
23 total AOD prediction when compared with MERRA-2 reanalysis during the period of July to November 2019. Though there  
24 are still some high biases over southern African fire region and eastern Asia and low biases over south America and dust  
25 source regions, GEFS-Aerosols reproduces the prominent temporal and geographical features of AOD as represented by  
26 satellite observations and reanalysis data, like dust plumes over North Africa and the Arabian Peninsula, biomass burning  
27 plumes in Southern Hemisphere, South America, Northwestern America and Eastern Europe, polluted air over Eastern and  
28 Southern Asia, and high-altitude sea-salt bands. We also sampled the forecast total AOD of GEFS-Aerosols and NGACv2 in  
29 the same location as 60 AERONET sites, which are spread globally and represent different aerosol regimes, and compared  
30 their variations for the 7/5/19-11/30/19. Much higher correlation coefficients against AERONET data are indicated for the  
31 GEFS-Aerosols than those for NGACv2 globally, and are quite comparable to those of the ICAP-MME.

32 During the biomass burning events, GEFS-Aerosols captured major fires over southern Africa, Siberia, Central Amazon and  
33 Central South America much better than NGACv2. Part of the improvement may be due to the vertical transport by the

1 plume-rise module. Generally, the total AOD time series of GEFS-Aerosols predictions matches closely to those of ICAP  
2 and AERONET during most of the time from July to November 2019 at the AERONET sites over South America, except  
3 there are some minor under predictions of several highest AOD episodes. In contrast, NGACv2 substantially underpredicted  
4 almost throughout the whole period and almost entirely missed many high AOD events. For the southern African event, the  
5 GEFS-Aerosols predictions are able to capture the daily total AOD variations seen in the AERONET observations, even  
6 better than that of the ICAP total AOD at the sites near the fire source regions, though there are overpredictions at the sites in  
7 downwind areas, which may be due to the lack of removal process or uncertainties of fire emission in central and southern  
8 Africa. In contrast, the NGACv2 results show under prediction in total AOD forecast at most of the AERONET sites in this  
9 region.

10 Overall, the model predicts total AOD variation by GEFS-Aerosols indicates much better performance than that of NGACv2  
11 over western North Africa. Although GEFS-Aerosols shows reductions in dust emissions over the Saharan dust source, the  
12 correlations with observations from downwind AERONET sites in western Africa are improved over those for NGACv2.  
13 The largest biases and discrepancies of GEFS-Aerosols and NGACv2 are both indicated in the sites in Tajikistan, which may  
14 be associated with a missing dust source near this site for both models. Obviously, other than the updates in anthropogenic  
15 and fire emissions, the implementation of FENGSH dust scheme into GEFS-Aerosols also shows great improvements in the  
16 dust concentration and AOD predictions over the dust regions compared to that of the NGACv2, which was using the  
17 original GOCART dust scheme.

18 We also evaluated predicted aerosols concentrations with different resolution against the ATom-1 aircraft measurements  
19 from July to August 2016. Overall, predicted aerosol concentrations are quite comparable to the ATom-1 measurements  
20 along the flight tracks globally with ~25 km model resolution. The model shows good performance in reproducing vertical  
21 profiles of OC, BC, sulfate, dust and sea salt, and the location of fire plumes was captured well overall. Sulfate over the  
22 Pacific, southern and tropical Atlantic is significantly underpredicted, suggesting an underestimation in the oceanic sulfur  
23 sources, such as DMS. A clear trend in increased overprediction with altitude for BC suggests that further refinements in  
24 characterizing precipitation scavenging of aerosol in GEFS-Aerosols is needed, since this is the only loss process for BC  
25 other than surface deposition. Compared to NGACv2, the much better performance of dust vertical profile at high latitude  
26 over Atlantic may suggest that the dust removal processes (either dry or wet deposition) may be more accurate in GEFS-  
27 Aerosols. That may be partly associated with different atmospheric model and physical scheme version using in GEFS-  
28 Aerosols. The differences in large scale wet deposition and convective wet scavenging schemes between GEFS-Aerosols  
29 and NGACv2 may also contribute to the substantial improvements showing in GEFS-Aerosols prediction for both AOD and  
30 concentrations.

31 This paper overviews advances and challenges in model development for operational atmospheric aerosol predictions at  
32 NOAA. This implementation advanced the global aerosol forecast capability for NOAA and made a step forward toward  
33 developing a global aerosol data assimilation system. Currently, the assimilation of AOD based on satellite observations is  
34 under development to constrain aerosol distributions in the GEFS-Aerosols model. Initial testing shows promise for



1 improvement of predictions as well as limitations indicating the need for refinements in quality control, data assimilation  
2 impacts on aerosol composition and vertical distribution, as well as a need for bias correction of satellite observations. With  
3 bias and other errors substantially reduced in the GEFS-Aerosols, especially when it is equipped with an aerosol data  
4 assimilation system. Current, though the aerosol feedback from the aerosol components has not yet been included into the  
5 atmospheric model for direct and indirect radiative feedback, the model provides a good starting point from which to  
6 investigate at the impact on weather predictions out to sub-seasonal and seasonal scales when including the aerosol  
7 feedbacks on atmospheric system in the future plan.

## 8 **Code and data availability**

9 The GEFS-Aerosols v1 code and model configuration for aerosol forecast here are available at  
10 <https://doi.org/10.5281/zenodo.5655290>. ATom-1 data is publicly available at the Oak Ridge National Laboratory  
11 Distributed Active Archive Center: [https://daac.ornl.gov/ATOM/guides/ATOM\\_merge.html](https://daac.ornl.gov/ATOM/guides/ATOM_merge.html) (Wofsy et al., 2018).

## 12 **Author contribution**

13 Li Zhang and Raffaele Montuoro were the major developers of the GEFS-Aerosols model, including implementing and  
14 coupling the aerosol components to the FV3GFSv15 meteorological model. Stuart McKeen helped to process the  
15 anthropogenic emission and background input data, provided suggestions during the development of GEFS-Aerosols, and  
16 evaluated the model performance with ATom-1 observations. Barry Baker developed and implemented the FENGSHA dust  
17 scheme into GEFS-Aerosols. Partha Bhattacharjee helped to evaluate the GEFS-Aerosols real-time and operational  
18 predictions. Georg Grell provided oversight of the model development. Li Zhang and Judy Henderson developed the  
19 workflow for GEFS-Aerosols prediction and worked with Li Pan to perform and manage the real-time and retrospective  
20 forecasts. R. Ahmadov provided guidance on the implementation of the fire plume rise scheme. Shobha Kondragunta,  
21 Xiaoyang Zhang, and Fangjun Li provided the GBBEPx v3 data. The other co-authors provided help, suggestions and  
22 project management throughout the GEFS-Aerosols modeling system development. Li Zhang prepared the manuscript with  
23 contributions from all co-authors.

## 24 **Competing interests**

25 The authors declare that they have no conflict of interest.

## 26 **Acknowledgements**

1 Li Zhang, Raffaele Montuoro, Haiqin Li and Ravan Ahmadov were supported by funding from NOAA GSL Award Number  
2 NA17OAR4320101. This work was also supported by the UFS Research to Operations Medium Range Weather/Seasonal to  
3 Subseasonal Atmospheric Composition sub-project.

#### 4 **Reference**

- 5 Ahmadov R, Grell G, James E, Csiszar I, Tsidulko M, Pierce B, McKeen, S., Benjamin, S., Alexander, C., Pereira, G.,  
6 Freitas, S., Goldberg, M.: Using VIIRS Fire Radiative Power data to simulate biomass burning emissions, plume rise and  
7 smoke transport in a real-time air quality modeling system. 2017 Ieee International Geoscience and Remote Sensing  
8 Symposium. IEEE International Symposium on Geoscience and Remote Sensing IGARSS. New York: Ieee; p. 2806-8, 2017.
- 9 Bauer, S. E., Im, U., Mezuman, K., & Gao, C. Y.: Desert dust, industrialization, and agricultural fires: Health impacts of  
10 outdoor air pollution in Africa. *Journal of Geophysical Research: Atmospheres*, 124, 4104–4120.  
11 <https://doi.org/10.1029/2018JD029336>, 2019.
- 12 Benedetti, A., Reid, J.S. and Colarco, P.R.: International cooperative for aerosol prediction workshop on aerosol forecast  
13 verification. *Bulletin of the American Meteorological Society*, 92, ES48–ES53. <https://doi.org/10.1175/BAMS-D-11-11-00105.1>, 2011.
- 15 Bhattacharjee, P. S., Wang, J., Lu, C.-H., and Tallapragada, V.: The implementation of NEMS GFS Aerosol Component  
16 (NGAC) Version 2.0 for global multispecies forecasting at NOAA/NCEP – Part 2: Evaluation of aerosol optical thickness,  
17 *Geosci. Model Dev.*, 11, 2333–2351, <https://doi.org/10.5194/gmd-11-2333-2018>, 2018.
- 18 Bhattacharjee, P. S., Zhang, L., Baker, B., Pan, L., Montuoro, R., Grell A. G., and McQueen, J. Evaluation of Aerosol  
19 Optical Depth forecast from NOAA's Global Aerosol Forecast Model (GEFS-Aerosols). To be submitted. 2021.
- 20 Black, T. L., Abeles, J. A., Blake, B. T., Jovic, D., Rogers, E., Zhang, X., Aligo, E. A. , Dawson, L. C. , Lin, Y., Strobach,  
21 E. , Shafran, P. C., Carley, J. R.. A limited area modeling capability for the Finite-Volume Cubed-Sphere (FV3) dynamical  
22 core and comparison with a global two-way nest. *Journal of Advances in Modeling Earth Systems*, 13,  
23 e2021MS002483. <https://doi.org/10.1029/2021MS002483>, 2021.
- 24 Bloom, S., Silva, A. da, and Dee, D.: Documentation and validation of the Goddard Earth Observing System (GEOS) data  
25 assimilation system-version 4, 1–187 pp, 2005.
- 26 Bourgeois, I., Peischl, J., Thompson, C. R., Aikin, K. C., Campos, T., Clark, H., Commane, R., Daube, B., Diskin, G. W.,  
27 Elkins, J. W., Gao, R.-S., Gaudel, A., Hints, E. J., Johnson, B. J., Kivi, R., McKain, K., Moore, F. L., Parrish, D. D., Querel,  
28 R., Ray, E., Sánchez, R., Sweeney, C., Tarasick, D. W., Thompson, A. M., Thouret, V., Witte, J. C., Wofsy, S. C., and  
29 Ryerson, T. B.: Global-scale distribution of ozone in the remote troposphere from the ATom and HIPPO airborne field  
30 missions, *Atmos. Chem. Phys.*, 20, 10611–10635, <https://doi.org/10.5194/acp-20-10611-2020>, 2020.
- 31 Bozzo, A., Benedetti, A., Flemming, J., Kipling, Z., and Rémy, S.: An aerosol climatology for global models based on the  
32 tropospheric aerosol scheme in the Integrated Forecasting System of ECMWF, *Geosci. Model Dev.*, 13, 1007–1034,  
33 <https://doi.org/10.5194/gmd-13-1007-2020>, 2020.
- 34 Burnett, R., Chen, H., Szyszkowicz, M., Fann, N., Hubbell, B., Pope, C. A., Spte, J.S., Brauer, M., Cohen, A., Weichenthal,  
35 S., Coggins, J., Di, Q., Brunekreef, B., Frostad, F., Lim, S.S., Kan, H., Walker, K.d., Thurston, G.D., Hayes, R.b., Lim, C.C.,  
36 Turner, M. C., Jerrett, M., Krewski, D., Gapstur, S.M., Diver, W.R., Ostro, B., Goldberg, D., Crouse, D.L., Martin, R.V.,  
37 Peters, P., Pinault, L., Tjepkema, M., Donkelaar, A., Villeneuve, P.J., Miller, A.B., Yin, P., Zhou, M., Wang, L., Janssen  
38 N.A.H., Marra, M., Atkinson, R.W., Tsang, H., Thach, T.Q., Cannon, J.B., Allen, R.T., Hart, J.E., Laden, F., Cesaroni, G.,  
39 Forastisere, F., Weinmayr, G., Jaensch, A., Nagel, G., Concin, H., and Spadaro, J.V.: Global estimates of mortality  
40 associated with longterm exposure to outdoor fine particulate matter, *P. Natl. Acad. Sci. USA*, 115(38), 9592–9597,  
41 [doi:10.1073/pnas.1803222115](https://doi.org/10.1073/pnas.1803222115), 2018.

- 1 Chappell, A., and Webb, N. P.: Using albedo to reform wind erosion modelling, mapping and monitoring. *Aeolian Research*,  
2 23, 63–78. <https://doi.org/10.1016/j.aeolia.2016.09.006>, 2016.
- 3 Chen, J. M., Li, C. L., Ristovski, Z., Milic, A., Gu, Y. T., Islam, M. S., Wang, S. X., Hao, J. M., Zhang, H. F., He, C. R.,  
4 Guo, H., Fu, H. B., Miljevic, B., Morawska, L., Thai, P., Fat, L., Pereira, G., Ding, A. J., Huang, X., and Dumka, U. C.: A  
5 review of biomass burning: Emissions and impacts on air quality, health and climate in China, *Sci. Total Environ.*, 579,  
6 1000–1034, <https://doi.org/10.1016/j.scitotenv.2016.11.025>, 2017.
- 7 Chen, Q., Yin, Y., Jin, L.-J., Xiao, H., Zhu, S.-Ch.: The effect of aerosol layers on convective cloud microphysics and  
8 precipitation, *Atmos. Res.*, 101 (1-2), pp. 327–340 <http://doi.org/10.1016/j.atmosres.2011.03.007>, 2011.
- 9 Chin, M., Ginoux, P., Kinne, S., Torres, O., Holben, B., Duncan, B., Martin, R., Logan, J., Higurashi, A., and Nakajima, T.:  
10 Tropospheric aerosol optical thickness from the GOCART model and comparisons with satellite and Sun photometer  
11 measurements, *J. Atmos. Sci.*, 59, 461–483, 2002.
- 12 Chin, M., Rood, B. R., Lin, S.-J., Muller, F. J., and Thomson, M. A.: Atmospheric sulfur cycle in the global model  
13 GOCART: Model description and global properties, *J. Geophys. Res.*, 105, 24,671–24,687, 2000.
- 14 Choi, Y., Kanaya, Y., Takigawa, M., Zhu, C., Park, S.-M., Matsuki, A., Sadanaga, Y., Kim, S.-W., Pan, X., and Pisso, I.:  
15 Investigation of the wet removal rate of black carbon in East Asia: validation of a below- and in-cloud wet removal scheme  
16 in FLEXible PARTicle (FLEXPART) model v10.4, *Atmos. Chem. Phys.*, 20, 13655–13670, [https://doi.org/10.5194/acp-20-](https://doi.org/10.5194/acp-20-13655-2020)  
17 13655-2020, 2020.
- 18 Colarco, P. R., Kahn, R. A., Remer, L. A., and Levy, R. C.: Impact of satellite viewing-swath width on global and regional  
19 aerosol optical thickness statistics and trends, *Atmos. Meas. Tech.*, 7, 2313–2335, <https://doi.org/10.5194/amt-7-2313-2014>,  
20 2014.
- 21 Colarco, P., Benedetti, A., Reid, J. and Tanaka, T.: Using EOS data to improve aerosol forecasting: the International  
22 Cooperative for Aerosol Research (ICAP). *The Earth Observer*, 26, 14–19, 2014.
- 23 Colarco, P., da Silva, A., Chin, M., and Diehl, T.: Online simulations of global aerosol distributions in the NASA GEOS-4  
24 model and comparisons to satellite and ground-based aerosol optical depth, *J. Geophys. Res.*, 115, D14207,  
25 [doi:10.1029/2009JD012820](https://doi.org/10.1029/2009JD012820), 2010.
- 26 Darmenov, A. and da Silva, A.: The Quick Fire Emissions Dataset (QFED) – Documentation of versions 2.1, 2.2 and 2.4,  
27 NASA Technical Report Series on Global Modeling and Data As- simulation, NASA/TM-2015–104606, Vol. 38, 211 pp.,  
28 avail- able at: <http://citeseerx.ist.psu.edu/viewdoc/download?doi=10.1.1.406.7724&rep=rep1&type=pdf> (last access: 4 June  
29 2018), 2015.
- 30 Diehl, T., Heil, A., Chin, M., Pan, X., Streets, D., Schultz, M., and Kinne, S.: Anthropogenic, biomass burning, and volcanic  
31 emis- sions of black carbon, organic carbon, and SO<sub>2</sub> from 1980 to 2010 for hindcast model experiments, *Atmos. Chem.*  
32 *Phys. Dis- cuss.*, 12, 24895–24954, <https://doi.org/10.5194/acpd-12-24895-2012>, 2012.
- 33 Easter, R. C., Ghan, S. J., Zhang, Y., Saylor, R. D., Chapman, E. G., Laulainen, N. S., Abdul-Razzak, H., Leung, L. R., Bian,  
34 X., and Zaveri, R. A.: MIRAGE: Model Description and Evaluation of Aerosols and Trace Gases. *J. Geophys. Res.*, 109,  
35 D20210, [doi:10.1029/2004JD004571](https://doi.org/10.1029/2004JD004571), 2004.
- 36 Eck, T. F., Holben, B. N., Reid, J. S., Dubovik, O., Smirnov, A., O'Neill, N. T., Slutsker, I., and Kinne, S.: The wavelength  
37 dependence of the optical depth of biomass burning, urban and desert dust aerosols, *J. Geophys. Res.*, 104, 31333–31350,  
38 1999.
- 39 Fast, J. D., Gustafson Jr., I. W., Easter, C. R., Zaveri, A. R., Barnard, C. J., Chapman, G. E., Grell, A. G., and Peckham, E. S.:  
40 Evolution of ozone, particulates, and aerosol direct radiative forcing in the vicinity of Houston using a fully coupled  
41 meteorology-chemistry-aerosol model. *J. Geophys. Res.*, 111, D21305, [doi:10.1029/2005JD006721](https://doi.org/10.1029/2005JD006721), 2006.

1 Fécan, F., Marticorena, B. and Bergametti, G.: Parametrization of the increase of the aeolian erosion threshold wind friction  
2 velocity due to soil moisture for arid and semi-arid areas. *Annales Geophysicae* 17, 149–157,  
3 <https://doi.org/10.1007/s00585-999-0149-7>, 1998.

4 Flentje, H., Mattis, I., Kipling, Z., Rémy, S., and Thomas, W.: Evaluation of ECMWF IFS-AER (CAMS) operational  
5 forecasts during cycle 41r1–46r1 with calibrated ceilometer profiles over Germany, *Geosci. Model Dev.*, 14, 1721–1751,  
6 <https://doi.org/10.5194/gmd-14-1721-2021>, 2021.

7 Forkel, R., Werhahn, J., Buus Hansen, A., McKeen, S., Peckham, S., Grell, G., Suppan, P.: Effect of aerosol-radiation  
8 feedback on regional air qualityeacase study with WFR/Chem. *Atmos. Environ.* 53,  
9 202e211.<http://dx.doi.org/10.1016/j.atmosenv.2011.10.009>, 2012

10 Freitas, S. R., Longo, K. M., Alonso, M. F., Pirre, M., Marecal, V., Grell, G., Stockler, R., Mello, R. F., and Sánchez Gácita,  
11 M.: PREP-CHEM-SRC – 1.0: a preprocessor of trace gas and aerosol emission fields for regional and global atmospheric  
12 chemistry models, *Geosci. Model Dev.*, 4, 419–433, doi:10.5194/gmd-4-419-2011, 2011.

13 Freitas, S. R., Longo, K. M., Chatfield, R., Latham, D., Silva Dias, M. A. F., Andreae, M. O., Prins, E., Santos, J. C., Gielow,  
14 R., and Carvalho Jr., J. A.: Including the sub-grid scale plume rise of vegetation fires in low resolution atmospheric transport  
15 models, *Atmos. Chem. Phys.*, 7, 3385–3398, <https://doi.org/10.5194/acp-7-3385-2007>, 2007.

16 Froyd, K. D., Murphy, D. M., Brock, C. A., Campuzano-Jost, P., Dibb, J. E., Jimenez, J.-L., Kupc, A., Middlebrook, A. M.,  
17 Schill, G. P., Thornhill, K. L., Williamson, C. J., Wilson, J. C., and Ziemba, L. D.: A new method to quantify mineral dust  
18 and other aerosol species from aircraft platforms using single-particle mass spectrometry, *Atmos. Meas. Tech.*, 12, 6209–  
19 6239, <https://doi.org/10.5194/amt-12-6209-2019>, 2019.

20 Gelaro, R., McCarty, W., Suárez, M. J., Todling, R., Molod, A., Takacs, L., Randles, C. A., Darmenov, A., Bosilovich, M.  
21 G., Reichle, R., Wargan, K., Coy, L., Cullather, R., Draper, C., Akella, S., Buchard, V., Conaty, A., da Silva, A. M., Gu, W.,  
22 Kim, G., Koster, R., Lucchesi, D. Merkova, J. E., Nielsen, G. Partyka, G., Pawson, S., Putman, W., Rienecker, M., Schubert,  
23 S. D., Sienkiewicz, M., and Zhao, B.: The Modern-Era Retrospective Analysis for Research and Applications, Version 2  
24 (MERRA-2), *J. Climate*, 30, 5419–5454, <https://doi.org/10.1175/JCLI-D-16-0758.1>, 2017.

25 Gillette, D. A., Adams, J., Endo, A., Smith, D., and Kihl, R.: Threshold velocities for input of soil particles into the air by  
26 desert soils, *J. Geophys. Res.*, 85 (C10), 5621– 5630, doi:10.1029/JC085iC10p05621, 1980.

27 Gillette, D. A.: Threshold friction velocities for dust production for agricultural soils. *Journal of Geophysical Research*,  
28 93(D10), 12645–12662. <https://doi.org/10.1029/jd093id10p12645>, 1988.

29 Grell, G. A., Peckham, E. S., Schmitz, R., McKeen, A. S., Frost, G., Skamarock, W., and Eder, B.: Fully-coupled online  
30 chemistry within the WRF model. *Atmospheric Environment*, 39, 6957–6975, doi:10.1016/j.atmosenv.2005.04.027, 2005.

31 Grell, G., Freitas, S. R., Stuefer, M., and Fast, J.: Inclusion of biomass burning in WRF-Chem: impact of wildfires on  
32 weather forecasts, *Atmos. Chem. Phys.*, 11, 5289–5303, <https://doi.org/10.5194/acp-11-5289-2011>, 2011.

33 Hoesly, R. M., Smith, S. J., Feng, L., Klimont, Z., Janssens-Maenhout, G., Pitkanen, T., Seibert, J. J., Vu, L., Andres, R. J.,  
34 Bolt, R. M., Bond, T. C., Dawidowski, L., Kholod, N., Kurokawa, J.-I., Li, M., Liu, L., Lu, Z., Moura, M. C. P., O'Rourke, P.  
35 R., and Zhang, Q.: Historical (1750–2014) anthropogenic emissions of reactive gases and aerosols from the Community  
36 Emissions Data System (CEDS), *Geosci. Model Dev.*, 11, 369–408, <https://doi.org/10.5194/gmd-11-369-2018>, 2018.

37 Holben, B. N., Eck, T. F., Slutsker, I., Tanré, D., Buis, J. P., Setzer, A., Vermote, E., Reagan, J. A., Kaufman, Y. J.,  
38 Nakajima, T., Lavenu, F., Jankowiak, I., and Smirnov, A.: AERONET – A Federated instrument network and data archive  
39 for aerosol characterization, *Remote Sens. Environ.*, 66, 1–16, 1998.

40 Hollingsworth, A., Engelen, R. J., Textor, C., Benedetti, A., Boucher, O., Chevallier, F., Dethof, A., Elbern, H., Eskes, H.,  
41 Flemming, J., Granier, C., Kaiser, J. W., Morcrette, J.-J., Rayner, P., Peuch, V.-H., Rouil, L., Schultz, M. G., and Simmons,  
42 A. J.: Toward a Monitoring and Forecasting System For Atmospheric Composition: The GEMS Project, *B. Am. Meteorol.*  
43 *Soc.*, 89, 1147–1164, 2008.

1 Hsu, N. C., Jeong, M.-J., Bettenhausen, C., Sayer, A. M., Hansell, R., Seftor, C. S., Huang, J., and Tsay, S.-C.: Enhanced  
2 Deep Blue aerosol retrieval algorithm: The second generation, *J. Geophys. Res.-Atmos.*, 118, 9296–  
3 9315, <https://doi.org/10.1002/jgrd.50712>, 2013.

4 Jackson, J., Liu, H., Laszlo, I., Kondragunta, S., Remer, L. A., Huang, J., and Huang, H.-C.: Suomi-NPP VIIRS Aerosol  
5 Algorithms and Data Products, *J. Geophys. Res.*, 118, 12673–12689, <https://doi.org/10.1002/2013jd020449>, 2013.

6 Janssens-Maenhout, G., Crippa, M., Guizzardi, D., Dentener, F., Muntean, M., Pouliot, G., Keating, T., Zhang, Q.,  
7 Kurokawa, J., Wankmüller, R., Denier van der Gon, H., Kuenen, J. J. P., Klimont, Z., Frost, G., Darras, S., Koffi, B., and Li,  
8 M.: HTAP\_v2.2: a mosaic of regional and global emission grid maps for 2008 and 2010 to study hemispheric transport of air  
9 pollution, *Atmos. Chem. Phys.*, 15, 11411–11432, <https://doi.org/10.5194/acp-15-11411-2015>, 2015.

10 Janssens-Maenhout, G.: EDGARv4.1 Emission Time Series, European Commission, Joint Research Centre (JRC) [Dataset]  
11 PID, available at: <http://data.europa.eu/89h/jrc-edgar-emissiontimeseriesv41> (last access: 12 June 2018), 2010.

12 Levin, Z., and Cotton R. W.: Aerosol Pollution Impact on Precipitation, *Aerosol Pollution Impact on Precipitation: A*  
13 *Scientific Review*, 407 pp., Springer, New York, 2009.

14 Levy, R. C., Mattoo, S., Munchak, L. A., Remer, L. A., Sayer, A. M., Patadia, F., and Hsu, N. C.: The Collection 6 MODIS  
15 aerosol products over land and ocean, *Atmos. Meas. Tech.*, 6, 2989–3034, <https://doi.org/10.5194/amt-6-2989-2013>, 2013.

16 Liu, F., Zhang, Q., van der A, R. J., Zheng, B., Tong, D., Yan, L., Zheng, Y., and He, K.: Recent reduction  
17 in NO<sub>x</sub> emissions over China: synthesis of satellite observations and emission inventories, *Environ. Res. Lett.*, 11,  
18 114002, <https://doi.org/10.1088/1748-9326/11/11/114002>, 2016.

19 Liu, H., Remer, L. A., Huang, J., Huang, H.-C., Kondragunta, S., Laszlo, I., Oo, M., and Jackson, J. M.: Preliminary  
20 Evaluation of Suomi-NPP VIIRS Aerosol Optical Thickness, *J. Geophys. Res.*, 119, 3942–  
21 3962, <https://doi.org/10.1002/2013jd020360>, 2013.

22 Lu, C.-H., da Silva, A., Wang, J., Moorthi, S., Chin, M., Colarco, P., Tang, Y., Bhattacharjee, P. S., Chen, S.-P., Chuang, H.-  
23 Y., Juang, H.-M. H., McQueen, J., and Iredell, M.: The implementation of NEMS GFS Aerosol Component (NGAC)  
24 Version 1.0 for global dust forecasting at NOAA/NCEP, *Geosci. Model Dev.*, 9, 1905–1919, <https://doi.org/10.5194/gmd-9-1905-2016>, 2016.

26 Lu, S., Huang, H.-C., Hou, Y.-T., Tang, Y., McQueen, J., da Silva, A., Chin, M., Joseph, E., and Stockwell, W.:  
27 Development of NCEP Global Aerosol Forecasting System: an overview and its application for improving weather and air  
28 quality forecasts, in: *NATO Science for Peace and Security Series: Air Pollution Modelling and Its Application XX*,  
29 Springer Publications, Dordrecht, the Netherlands, 451–454, <https://doi.org/10.1007/978-90-481-3812-8>, 2010.

30 MacKinnon, D. J., Clow, G. D., Tigges, R. K., Reynolds, R. L., and Chaves Jr. P. S.: Comparison of aerodynamically and  
31 model-derived roughness lengths ( $z_0$ ) over diverse surfaces, central Mojave Desert, California, USA, *Geomorphology*, 63,  
32 103–113, doi:10.1016/j.geomorph.2004.03.009, 2004

33 Marticorena, B. and Bergametti, G.: Modeling the atmospheric dust cycle: 1-Design of a soil derived dust production scheme,  
34 *J. Geophys. Res.*, 100, 16415–16430, 1995.

35 Molod, A., Takacs, L., Suarez, M., and Bacmeister, J.: Development of the GEOS-5 atmospheric general circulation model:  
36 evolution from MERRA to MERRA2, *Geosci. Model Dev.*, 8, 1339–1356, <https://doi.org/10.5194/gmd-8-1339-2015>, 2015.

37 Morcrette, J.-J., Beljaars, A., Benedetti, A., Jones, L. and Boucher, O.: Sea-salt and dust aerosols in the ECMWF IFS model.  
38 *Geophysical Research Letters*, 35, L24813, 2008.

39 Muhlbauer, A., Grabowski, W. W., Malinowski, P. S., Ackerman, P. T., Bryan, H. G., Lebo, J. Z., Milbrandt, A. J., Morrison,  
40 H., Ovchinnikov, M., Tessendorf, S., Thériault, G. J.M.: Thompson Reexamination of the state of the art of cloud modelling  
41 shows real improvements, *Bull. Am. Meteorol. Soc.*, 94, pp. ES45–ES48, <http://doi.org/10.1175/BAMS-D-12-00188.1>,  
42 2013.

- 1 Mulcahy, J. P., Walters, D. N., Bellouin, N., and Milton, S. F.: Impacts of increasing the aerosol complexity in the Met  
2 Office global numerical weather prediction model, *Atmos. Chem. Phys.*, 14, 4749-4778, doi:10.5194/acp-14-4749-2014,  
3 2014.
- 4 Murphy, D. M., Froyd, K. D., Bian, H., Brock, C. A., Dibb, J. E., DiGangi, J. P., Diskin, G., Dollner, M., Kupc, A., Scheuer,  
5 E. M., Schill, G. P., Weinzierl, B., Williamson, C. J., and Yu, P.: The distribution of sea-salt aerosol in the global  
6 troposphere, *Atmos. Chem. Phys.*, 19, 4093–4104, <https://doi.org/10.5194/acp-19-4093-2019>, 2019.
- 7 Murphy, D., Froyd, K., Apel, E., Blake, R. D., Blake, J. N., Evangeliou, N., Hornbrook, S. R., Peischl, J., Ray, E., Ryerson, B.  
8 T., Thompson, C., and Stohl, A.: An aerosol particle containing enriched uranium encountered in the remote T upper  
9 troposphere, *J. Environ. Radioactivity*, 184–185, 95-100, doi:10.1016/j.jenvrad.2018.01.006, 2018
- 10 Owen, P. R.: Saltation of uniform grains in air. *Journal of Fluid Mechanics*, 20(2), 225–242.  
11 <https://doi.org/10.1017/S0022112064001173>, 1964.
- 12 Powers, J. G., Klemp, J. B., Skamarock, W. C., Davis, C. A., Dudhia, J., Gill, D. O., Coen, J. L., Gochis, D. J., Ahmadov, R.,  
13 Peckham, S. E., Grell, G. A., Michalakes, J., Trahan, S., Benjamin, S. G., Alexander, C. R., Dimego, G. J., Wang, W.,  
14 Schwartz, C. S., Romine, G. S., Liu, Z., Snyder, C., Chen, F., Barlage, M. J., Yu, W., & Duda, M. G. : The Weather  
15 Research and Forecasting Model: Overview, System Efforts, and Future Directions, *Bulletin of the American Meteorological*  
16 *Society*, 98(8), 1717-1737, 2017.
- 17 Prigent, C., Jiménez, C., and Catherinot, J.: Comparison of satellite microwave backscattering (ASCAT) and visible/near-  
18 infrared reflectances (PARASOL) for the estimation of aeolian aerodynamic roughness length in arid and semi-arid regions,  
19 *Atmos. Meas. Tech.*, 5, 2703–2712, <https://doi.org/10.5194/amt-5-2703-2012>, 2012.
- 20 Raupach, M. R.: Drag and drag partition on rough surfaces. *Boundary-Layer Meteorology*.  
21 <https://doi.org/10.1007/BF00155203>, 1992.
- 22 Reale, O., Lau, K. M., and Silva da, A.: Impact of interactive aerosol on the African easterly jet in the NASA GEOS-5  
23 Global Forecasting System. *Wea. Forecasting*, 26, 504–519, 2011.
- 24 Reid, J., Benedetti, A., Colarco, P. R., and Hansen, J. A.: International operational aerosol observability work-shop, *B. Am.*  
25 *Meteorol. Soc.*, 92, ES21-ES24, <https://doi.org/10.1175/2010BAMS3183.1>, 2011.
- 26 Rienecker, M.M., Suarez, M.J., Todling, R., Bacmeister, J., Takacs, L., Liu, H.-C., Gu, W., Sienkiewicz, M., Koster, R.D.,  
27 Gelaro, R., Stajner, I. and Nielsen, J.E.: The GEOS-5 data assimilation system: documentation of versions 5.0.1, 5.1.0, and  
28 5.2.0., Suarez, M.J. (ed.). NASA Tech. Memo. 2008-104606, Vol. 27, 2008.
- 29 Rodwell, M. J. and Jung, T.: Understanding the local and global impacts of model physics changes: an aerosol example,  
30 *Q.J.R. Meteorol. Soc.*, 134, 1479–1497, doi:10.1002/qj.298, 2008.
- 31 Sayer, A. M., Hsu, N. C., Bettenhausen, C., and Jeong, M.-J.: Validation and uncertainty estimates for MODIS Collection 6  
32 “Deep Blue” aerosol data, *J. Geophys. Res.-Atmos.*, 118, 7864–7872, <https://doi.org/10.1002/jgrd.50600>, 2013.
- 33 Sayer, A. M., Munchak, L. A., Hsu, N. C., Levy, R. C., Bettenhausen, C., and Jeong M.-J.: MODIS Collection 6 aerosol  
34 products: Comparison between Aqua's e-Deep blue, dark target and “merged” data sets and usage recommendations,  
35 *J. Geophys. Res.-Atmos.*, 119, 13965–989, 2014.
- 36 Schill, G.P., Froyd, K.D., Bian, H., Kupc, A., Williamson, C., Brock, C. A., Ray, E., Hornbrook, R. S., Hills, A. J., Apel, E.  
37 C., Chin, M., Colarco, P. R., Murphy, D. M.: Widespread biomass burning smoke throughout the remote troposphere. *Nat.*  
38 *Geosci.* 13, 422–4. <https://doi.org/10.1038/s41561-020-0586-1>, 2020
- 39 Sessions, W. R., Reid, J. S., Benedetti, A., Colarco, P. R., da Silva, A., Lu, S., Sekiyama, T., Tanaka, T. Y., Baldasano, J. M.,  
40 Basart, S., Brooks, M. E., Eck, T. F., Iredell, M., Hansen, J. A., Jorba, O. C., Juang, H.-M. H., Lynch, P., Morcrette, J.-J.,  
41 Moorthi, S., Mulcahy, J., Pradhan, Y., Razinger, M., Sampson, C. B., Wang, J., and Westphal, D. L.: Development towards a  
42 global operational aerosol consensus: basic climatological characteristics of the International Cooperative for Aerosol

1 Prediction Multi-Model Ensemble (ICAP-MME), *Atmos. Chem. Phys.*, 15, 335–362, [https://doi.org/10.5194/acp-15-335-](https://doi.org/10.5194/acp-15-335-2015)  
2 [2015](https://doi.org/10.5194/acp-15-335-2015), 2015

3 Shao, Y., Ishizuka, M., Mikami, M., and Leys, J. F.: Parameterization of size-resolved dust emission and validation with  
4 measurements. *Journal of Geophysical Research Atmospheres*, 116(8), D08203. <https://doi.org/10.1029/2010JD014527>,  
5 2011.

6 Shao, Y., Raupach, M. R., and Findlater, P. A.: Effect of saltation bombardment on the entrainment of dust by wind. *Journal*  
7 *of Geophysical Research*, 98(D7), 12719–12726. <https://doi.org/10.1029/93jd00396>, 1993.

8 Shi, X., and Brasseur, G. P.: The response in air quality to the reduction of Chinese economic activities during the  
9 COVID-19 outbreak. *Geophysical Research Letters*, 47, e2020GL088070. <https://doi.org/10.1029/2020GL088070>, 2020.

10 Slinn, W. G. N.: Precipitation scavenging, in *Atmospheric Science and Power Production*, edited by: D. Randerson, U.S.  
11 Dept. of Energy, Washington D. C., 472–477, 1984.

12 Theurich, G., DeLuca, C., Campbell, T., Liu, F., Saint, K., Vertenstein, M., Chen, J., Oehmke, R., Doyle, J., Whitcomb, T.,  
13 Wallcraft, A., Iredell, M., Black, T., da Silva, A.M., Clune, T., Ferraro, R., Li, P., Kelley, M., Aleinov, I., Balaji, V., Zadeh,  
14 N., Jacob, R., Kirtman, B., Giraldo, F., McCarren, D., Sandgathe, S., Peckham, S., and Dunlap, IV, R.: The Earth System  
15 Prediction Suite: Toward a coordinated U.S. modeling capability. *Bull. Amer. Meteorol. Soc.*, 97, no. 7, 1229-1247,  
16 doi:10.1175/BAMS-D-14-00164.1, 2016.

17 Thomson, D.S., Schein, M. E., Murphy, D.M.: Particle analysis by laser mass spectrometry WB-57F instrument overview.  
18 *Aero. Sci. Technol.* 33, 153–169, 2000.

19 Tong, D. Q., Wang, J. X. L., Gill, T. E., Lei, H., and Wang, B.: Intensified dust storm activity and Valley fever infection in  
20 the southwestern United States, *Geophys. Res. Lett.*, 44, 4304– 4312, doi:10.1002/2017GL073524, 2017.

21 Wang Q, Su M.: A preliminary assessment of the impact of COVID-19 on environment—a case study of China. *Sci Total*  
22 *Environ*, 728:138915. doi: 10.1016/j.scitotenv.2020.138915, 2020.

23 Wang, H., Rasch, J. P., Easter, C. R., Singh, B., Zhang, R., Ma, P.-L., Qian, Y., Ghan, J. S., and Beagley, N.: Using an  
24 explicit emission tagging method in global modeling of source receptor relationships for black carbon in the Arctic:  
25 Variations, sources, and transport pathways, *J. Geophys. Res. Atmos.*, 119, 12,888–12,909, doi:10.1002/2014JD022297,  
26 2014.

27 Wang, J., Bhattacharjee, P. S., Tallapragada, V., Lu, C.-H., Kondragunta, S., da Silva, A., Zhang, X., Chen, S.-P., Wei, S.-  
28 W., Darmenov, A. S., McQueen, J., Lee, P., Koner, P., and Harris, A.: The implementation of NEMS GFS Aerosol  
29 Component (NGAC) Version 2.0 for global multispecies forecasting at NOAA/NCEP – Part 1: Model descriptions, *Geosci.*  
30 *Model Dev.*, 11, 2315–2332, <https://doi.org/10.5194/gmd-11-2315-2018>, 2018.

31 Wang, Q., Jacob, J. D., Spackman, R. J., Perring, E. A., Schwarz, P. J., Moteki, N., Marais, A. E., Ge, C., Wang, J., and  
32 Barrett, R. H. S.: Global budget and radiative forcing of black carbon aerosol: Constraints from pole-to-pole (HIPPO)  
33 observations across the Pacific, *J. Geophys. Res. Atmos.*, 119, 195–206, doi:10.1002/2013JD020824, 2014.

34 Wofsy, S. C., Afshar, S., Allen, H. M., Apel, E., Asher, E. C., Barletta, B., Bent, J., Bian, H., Biggs, B. C., Blake, D. R.,  
35 Blake, N., Bourgeois, I., Brock, C. A., Brune, W. H., Budney, J. W., Bui, T. P., Butler, A., Campuzano-Jost, P., Chang, C. S.,  
36 Chin, M., Commane, R., Correa, G., Crounse, J. D., Cullis, P. D., Daube, B. C., Day, D. A., Dean-Day, J. M., Dibb, J. E.,  
37 Di-Gangi, J. P., Diskin, G. S., Dollner, M., Elkins, J. W., Erdesz, F., Fiore, A. M., Flynn, C. M., Froyd, K., Gesler, D. W.,  
38 Hall, S. R., Hanisco, T. F., Hannun, R. A., Hills, A. J., Hintsa, E. J., Hoffman, A., Hornbrook, R. S., Huey, L. G., Hughes, S.,  
39 Jimenez, J. L., Johnson, B. J., Katich, J. M., Keeling, R. F., Kim, M. J., Kupc, A., Lait, L. R., Lamarque, J.-F., Liu, J.,  
40 McKain, K., Mclaughlin, R. J., Meinardi, S., Miller, D. O., Montzka, S. A., Moore, F. L., Morgan, E. J., Murphy, D. M.,  
41 Murray, L. T., Nault, B. A., Neuman, J. A., Newman, P. A., Nicely, J. M., Pan, X., Paplawsky, W., Peischl, J., Prather, M. J.,  
42 Price, D. J., Ray, E., Reeves, J. M., Richardson, M., Rollins, A. W., Rosenlof, K. H., Ryerson, T. B., Scheuer, E., Schill, G.  
43 P., Schroder, J. C., Schwarz, J. P., St.Clair, J. M., Steenrod, S. D., Stephens, B. B., Strode, S. A., Sweeney, C., Tanner, D.,  
44 Teng, A. P., Thames, A. B., Thompson, C. R., Ullmann, K., Veres, P. R., Vieznor, N., Wagner, N. L., Watt, A., Weber, R.,

- 1 Weinzierl, B., Wennberg, P., Williamson, C. J., Wilson, J. C., Wolfe, G. M., Woods, C. T., and Zeng, L. H.: ATom: Merged  
 2 Atmospheric Chemistry, Trace Gases, and Aerosols, ORNL DAAC, Oak Ridge, Tennessee,  
 3 <https://doi.org/10.3334/ornl daac/1581>, 2018.
- 4 Xian, P., Reid, J. S., Hyer, E. J., Sampson, C. R., Rubin, J. I., Ades, M., Asencio, N., Basart, S., Benedetti, A., Bhattacharjee,  
 5 P. S., Brooks, M. E., Colarco, P. R., da Silva, A. M., Eck, T. F., Guth, J., Jorba, O.I., Kouznetsov, R., Kipling, Z., Sofiev, M.,  
 6 Garcia-Pando, C. P., Pradhan, Y., Tanaka, T., Wang, J., Westphal, D. L., Yumimoto, K., Zhang J.: Current state of the global  
 7 operational aerosol multi-model ensemble: An update from the International Cooperative for Aerosol Prediction (ICAP). Q.  
 8 J. R. Meteorol. Soc.; 145 ( Suppl. 1): 176– 209. <https://doi.org/10.1002/qj.3497>, 2019.
- 9 Xie, S. P., B. Lu, and Xiang, Q. B.: Similar spatial patterns of climate responses to aerosol and greenhouse gas changes. Nat.  
 10 Geosci., 6, 828–832, doi:<https://doi.org/10.1038/ngeo1931>, 2013.
- 11 Xing, J., Li, S., Jiang, Y., Wang, S., Ding, D., Dong, Z., Zhu, Y., and Hao, J.: Quantifying the emission changes and  
 12 associated air quality impacts during the COVID-19 pandemic on the North China Plain: a response modeling study, Atmos.  
 13 Chem. Phys., 20, 14347–14359, <https://doi.org/10.5194/acp-20-14347-2020>, 2020.
- 14 Yang, Q., Bitz, C. M., and Doherty, S. J.: Offsetting effects of aerosols on Arctic and global climate in the late 20th century,  
 15 Atmos. Chem. Phys., 14, 3969-3975, <https://doi.org/10.5194/acp-14-3969-2014>, 2014.
- 16 Zhang, L., Grell, G. A., McKeen, S. A., Ahmadov, R., Froyd, K. D., and Murphy, D.: Inline coupling of simple and complex  
 17 chemistry modules within the global weather forecast model FIM (FIM-Chem v1), Geosci. Model Dev., 15, 467–491,  
 18 <https://doi.org/10.5194/gmd-15-467-2022>, 2022.
- 19 Zhang, Q., He, K., and Huo, H.: Cleaning China's air, Nature, 484, 161–162, <https://doi.org/10.1038/484161a>, 2012.
- 20 Zhang, X., Kondragunta, S., da Silva, A., Lu, S., Ding, H., Li, F., and Zhu, Y.: The blended global biomass burning  
 21 emissions product from MODIS and geostationary satellites (GBBEPx), [http://www.ospo.noaa.gov/Products/land/  
 22 gbbepx/docs/GBBEPx\\_ATBD.pdf](http://www.ospo.noaa.gov/Products/land/gbbepx/docs/GBBEPx_ATBD.pdf) (last access: 1 June 2018), 2014.
- 23 Zhang, X., Kondragunta, S., Ram, J., Schmidt, C., and Huang, H.-C.: Near-real-time global biomass burning emissions  
 24 product from geostationary satellite constellation, J. Geophys. Res., 117, D14201, <https://doi.org/10.1029/2012JD017459>,  
 25 2012.
- 26 Zhao, T. X., Stowe, L. L., Smirnov, A., Crosby, D., Sapper, J., and McClain, C. R.: Development of a global validation  
 27 package for satellite oceanic aerosol optical thickness retrieval based on AERONET observations and its application to  
 28 NOAA/NESDIS operational aerosol retrievals, J. Atmos. Sci., 59, 294–312, 2002.

29

30 **Table.**

31 **Table 1.** AERONET site information, the correlation coefficients and root mean square error (RMSE) of GEFS-Aerosols,  
 32 ICAP and NGACv2 AOD with respect to that of AERONET observation for the period 7/5/2019-11/30/2019.  
 33 Correlation coefficients are at the 95% confidence interval.

34

| Stations | Station Names | (Latitude, Longitude) | Corr. with<br>GEFS-<br>Aerosols | Corr. with<br>NGACv2 | Corr. with<br>ICAP | RMSE with<br>GEFS-<br>Aerosols | RMSE with<br>NGACv2 | RMSE with<br>ICAP |
|----------|---------------|-----------------------|---------------------------------|----------------------|--------------------|--------------------------------|---------------------|-------------------|
| 1        | Dakar         | (14.39N, 16.95W)      | 0.60                            | 0.21                 | 0.78               | 0.19                           | 0.24                | 0.10              |
| 2        | Cape Verde    | (16.73N, 22.93W)      | 0.54                            | 0.39                 | 0.86               | 0.25                           | 0.27                | 0.11              |
| 3        | Banizoumbu    | (13.54N, 2.66E)       | 0.46                            | 0.23                 | 0.81               | 0.19                           | 0.25                | 0.14              |
| 4        | Tamanrassett  | (22.79N, 5.53E)       | 0.40                            | 0.29                 | 0.78               | 0.26                           | 0.34                | 0.17              |
| 5        | Tenerife      | (28.47N, 16.24W)      | 0.55                            | 0.32                 | 0.88               | 0.17                           | 0.19                | 0.06              |



|    |                    |                  |      |      |      |      |      |      |
|----|--------------------|------------------|------|------|------|------|------|------|
| 6  | Saada              | (31.62N, 8.15W)  | 0.72 | 0.17 | 0.83 | 0.19 | 0.30 | 0.10 |
| 7  | Ben Salem          | (35.55N, 9.91E)  | 0.74 | 0.15 | 0.86 | 0.08 | 0.29 | 0.07 |
| 8  | Sede Boker         | (30.85N, 34.78E) | 0.72 | 0.16 | 0.83 | 0.10 | 0.20 | 0.07 |
| 9  | Dewa               | (24.76N, 55.36E) | 0.47 | 0.41 | 0.85 | 0.29 | 0.30 | 0.13 |
| 10 | Granada            | (37.16N, 3.60W)  | 0.82 | 0.32 | 0.77 | 0.08 | 0.13 | 0.08 |
| 11 | Cape San Juan      | (18.38N, 65.62W) | 0.43 | 0.28 | 0.64 | 0.14 | 0.21 | 0.04 |
| 12 | Dushanbe           | (38.55N, 68.85E) | 0.29 | 0.14 | 0.60 | 0.32 | 0.33 | 0.25 |
| 13 | Dalanzadgaad       | (43.57N,104.41E) | 0.71 | 0.46 | 0.81 | 0.13 | 0.16 | 0.10 |
| 14 | Beijing            | (39.97N,116.38E) | 0.67 | 0.47 | 0.80 | 0.43 | 0.68 | 0.33 |
| 15 | Kanpur             | (26.51N, 80.23E) | 0.76 | 0.15 | 0.87 | 0.36 | 0.51 | 0.32 |
| 16 | Kyiv               | (50.36N, 30.49E) | 0.45 | 0.18 | 0.62 | 0.14 | 0.20 | 0.06 |
| 17 | Barcelona          | (41.38N, 2.11E)  | 0.62 | 0.39 | 0.76 | 0.12 | 0.16 | 0.08 |
| 18 | Leipzig            | (51.35N, 12.43E) | 0.77 | 0.20 | 0.80 | 0.11 | 0.13 | 0.05 |
| 19 | Sochengcho         | (37.42N,124.73E) | 0.63 | 0.63 | 0.74 | 0.31 | 0.47 | 0.24 |
| 20 | Singapore          | (1.29N,103.78E)  | 0.40 | 0.19 | 0.62 | 0.66 | 0.89 | 0.36 |
| 21 | Reunion St Denis   | (20.90S, 55.48E) | 0.42 | 0.46 | 0.74 | 0.05 | 0.08 | 0.05 |
| 22 | Lumbini            | (27.50N, 83.28E) | 0.44 | 0.32 | 0.58 | 0.28 | 0.29 | 0.29 |
| 23 | Cape Fuguei        | (25.29N,121.53E) | 0.66 | 0.33 | 0.63 | 0.37 | 0.66 | 0.34 |
| 24 | Lake Argyle        | (16.10S,128.74E) | 0.60 | 0.37 | 0.78 | 0.06 | 0.06 | 0.05 |
| 25 | Chilbolton         | (51.14N, 1.43W)  | 0.66 | 0.20 | 0.79 | 0.09 | 0.12 | 0.05 |
| 26 | Opal               | (79.99N, 85.93W) | 0.19 | 0.13 | 0.61 | 0.12 | 0.16 | 0.08 |
| 27 | Resolute Bay       | (74.70N, 94.96W) | 0.28 | 0.21 | 0.62 | 0.11 | 0.11 | 0.06 |
| 28 | Thule              | (76.51N, 68.76W) | 0.32 | 0.13 | 0.57 | 0.12 | 0.13 | 0.07 |
| 29 | Kangerlussuaq      | (66.99N, 50.62W) | 0.83 | 0.35 | 0.97 | 0.09 | 0.10 | 0.05 |
| 30 | Tomsk              | (56.45N, 85.04E) | 0.72 | 0.18 | 0.83 | 0.55 | 0.79 | 0.27 |
| 31 | Hornsund           | (77.0N, 15.54E)  | 0.66 | 0.68 | 0.90 | 0.13 | 0.16 | 0.07 |
| 32 | Alta Floresta      | (9.87S, 56.10W)  | 0.81 | 0.30 | 0.88 | 0.24 | 0.34 | 0.12 |
| 33 | Santa Cruz Utepsa  | (17.76S, 63.20W) | 0.86 | 0.45 | 0.94 | 0.21 | 0.42 | 0.13 |
| 34 | Itajuba            | (22.41S, 45.45W) | 0.43 | 0.25 | 0.57 | 0.17 | 0.24 | 0.09 |
| 35 | La Paz             | (16.53S, 68.06W) | 0.48 | 0.19 | 0.79 | 0.07 | 0.12 | 0.08 |
| 36 | SEGS Lope Gabon    | (0.202S, 11.60E) | 0.71 | 0.43 | 0.94 | 0.29 | 0.69 | 0.39 |
| 37 | Ascension Island   | (7.97S, 14.41W)  | 0.54 | 0.45 | 0.33 | 0.13 | 0.25 | 0.08 |
| 38 | Bamenda            | (5.94N, 10.15E)  | 0.67 | 0.59 | 0.94 | 0.17 | 0.17 | 0.47 |
| 39 | Mongu Inn          | (15.26S, 23.13E) | 0.72 | 0.15 | 0.86 | 0.17 | 0.32 | 0.17 |
| 40 | Misamfu            | (10.17S, 31.22E) | 0.80 | 0.38 | 0.83 | 0.17 | 0.35 | 0.15 |
| 41 | Maun Tower         | (19.9S, 23.55E)  | 0.66 | 0.26 | 0.85 | 0.10 | 0.22 | 0.11 |
| 42 | Windpoort          | (19.36S, 15.48E) | 0.64 | 0.33 | 0.69 | 0.18 | 0.29 | 0.09 |
| 43 | Lubango            | (14.95S, 13.44E) | 0.81 | 0.72 | 0.54 | 0.16 | 0.32 | 0.14 |
| 44 | Bonanza Creek      | (64.74N,148.31W) | 0.77 | 0.21 | 0.70 | 0.32 | 0.60 | 0.23 |
| 45 | Fort McMurray      | (56.75N,111.47W) | 0.72 | 0.14 | 0.71 | 0.16 | 0.29 | 0.12 |
| 46 | Chapais            | (49.82N, 74.97W) | 0.32 | 0.11 | 0.55 | 0.11 | 0.14 | 0.07 |
| 47 | Saturn Island      | (48.77N,123.12W) | 0.63 | 0.28 | 0.76 | 0.09 | 0.09 | 0.05 |
| 48 | Missoula           | (46.91N,114.08W) | 0.43 | 0.14 | 0.79 | 0.09 | 0.11 | 0.04 |
| 49 | Camaguey           | (21.42N, 77.85W) | 0.63 | 0.16 | 0.82 | 0.06 | 0.12 | 0.04 |
| 50 | Neon Wood          | (47.12N, 99.24W) | 0.58 | 0.18 | 0.75 | 0.10 | 0.16 | 0.06 |
| 51 | GSFC               | (38.99N, 76.84W) | 0.47 | 0.15 | 0.77 | 0.08 | 0.16 | 0.06 |
| 52 | Monterey           | (36.59N,121.85W) | 0.39 | 0.32 | 0.66 | 0.04 | 0.04 | 0.03 |
| 53 | Toronto            | (43.79N, 79.47W) | 0.66 | 0.17 | 0.52 | 0.15 | 0.19 | 0.10 |
| 54 | Red Mountain Pass  | (37.90N,107.71W) | 0.65 | 0.15 | 0.76 | 0.03 | 0.04 | 0.02 |
| 55 | Tucson             | (32.23N,110.95W) | 0.62 | 0.16 | 0.81 | 0.05 | 0.08 | 0.03 |
| 56 | Appalachian State  | (36.21N, 81.69W) | 0.69 | 0.11 | 0.75 | 0.07 | 0.13 | 0.05 |
| 57 | Cartel             | (45.38N, 71.93W) | 0.08 | 0.19 | 0.26 | 0.09 | 0.13 | 0.06 |
| 58 | Mauna Loa          | (19.53N,155.57W) | 0.35 | 0.20 | 0.79 | 0.05 | 0.04 | 0.04 |
| 59 | ARM SGP            | (36.6N, 97.48W)  | 0.64 | 0.26 | 0.64 | 0.08 | 0.14 | 0.05 |
| 60 | Univ. of Wisconsin | (43.07N, 89.41W) | 0.60 | 0.21 | 0.78 | 0.06 | 0.08 | 0.05 |

1  
2

3 **Table 2.** Comparison of model configurations between GEFS-Aerosols and NGACv2

| Mode Configurations                             | GEFS-Aerosols        | NGACv2                      |
|-------------------------------------------------|----------------------|-----------------------------|
| Atmospheric model                               | FV3                  | NEMS GSM                    |
| Physics package                                 | GFS v15 (2019)       | GFS v2015 (2015)            |
| Horizontal resolution                           | ~25 km               | ~100 km                     |
| Vertical resolution                             | 64 layers            | 64 layers                   |
| Coupled infrastructure                          | NUOPC                | ESMF                        |
| Anthropogenic Emission                          | CEDS 2014            | EDGAR v4.1                  |
| Fire Emission                                   | GBBEPx v3            | GBBEPx [Zhang et al., 2014] |
| Aerosol scheme for BC, OC, sulfate and sea salt | GOCART from WRF-Chem | GOCART from GEOS-5          |
| Dust scheme                                     | FENGSHA              | GOCART                      |

4  
5  
6  
7

**Table 3.** ATom-1 and GEFS-Aerosols column sum statistics of mean bias and correlation for sulfate, OC, EC and dust.

| Species             | N   | Obs. median (mg/m <sup>2</sup> ) | GEFS-Aerosols MMO | NGACv2 MMO | GEFS-Aerosols r-coefficient | NGACv2 r-coefficient |
|---------------------|-----|----------------------------------|-------------------|------------|-----------------------------|----------------------|
| Sulfate             | 153 | 0.58                             | 0.72              | -          | 0.63                        | -                    |
| OC                  | 146 | 0.55                             | 1.03              | -          | 0.80                        | -                    |
| BC                  | 152 | 0.011                            | 3.35              | -          | 0.78                        | -                    |
| Dust (< 3. μm diam) | 130 | 0.038                            | 0.54              | 46.37      | 0.39                        | 0.39                 |

8 N is the sample number, MMO stands for Median Model to Observed Ratio, and r-coefficient is the Pearson correlation r-  
9 coefficient.

10

11 **Figure Captions.**

12 **Figure 1.** Diagram showing the components within the NEMS infrastructure.

13 **Figure 2.** (a) Diagram of GEFS-Aerosols coupled structure; (b) Flowchart of steps/tasks for GEFS-Aerosols in the global  
14 workflow forecast system.

15 **Figure 3.** Anthropogenic emissions of CEDS (2014) and HTAP (2010) for SO<sub>2</sub> (mole/km<sup>2</sup>/hr), BC and OC (ng/m<sup>2</sup>/s) on  
16 summer of July.

1 **Figure 4.** Total AOD forecast on 25th August compared with the NGACv2 model, MERRA2 reanalysis data and satellite  
2 observations of VIIRS and MODIS. The 18z forecasts from both models for that day and daily satellite data are used in the  
3 figure. Satellite data gaps are in white.

4 **Figure 5.** Correlation coefficients and RMSE between AERONET daily total AOD observations and GEFS-Aerosols, ICAP  
5 and NGACv2 for the period 7/5/19-11/30/19. Correlation coefficients are at the 95% confidence interval.

6 **Figure 6.** Day 1 AOD prediction averaged during 7/5/19-11/30/19 of GEFS-Aerosols and NGACv2 compared with  
7 MERRA-2 reanalysis and MODIS.

8 **Figure 7.** Day 1 AOD forecast biases of GEFS-Aerosols and NGACv2 compared with MERRA-2 averaged during 7/5/19-  
9 11/30/19 for dust, OC and sulfate.

10 **Figure 8.** Differences of GEFS-Aerosols and NGACv2 Day 1 predictions of total AOD compared with MERRA-2  
11 reanalysis averaged during 7/5/19-11/30/19.

12 **Figure 9.** Day 1 AOD forecasts of GEFS-Aerosols, ICAP, and NGACv2 verified against AERONET sites in South America  
13 during 7/5/19-11/30/19.

14 **Figure 10.** Day 1 AOD forecasts of GEFS-Aerosols, ICAP, and NGACv2 verified against AERONET sites in Africa during  
15 7/5/19-11/30/19.

16 **Figure 11.** Day 1 AOD forecasts of GEFS-Aerosols, ICAP, and NGACv2 verified against AERONET sites in dust source  
17 regions and surrounding downwind areas during 7/5/19-11/30/19.

18 **Figure 12.** Daily AERONET total AOD versus modeled total AOD from GEFS-Aerosols (blue) and NGACv2 (orange) at  
19 the AERONET sites of (a) Tamanrasset, (b) Cape Verde, and (c) Tenerife with linear regression fits.

20 **Figure 13.** GEFS-Aerosols and NGACv2 day 1 total AOD forecast time series against MERRA-2 reanalysis data averaged  
21 over major global regions of North Africa (0°-35°N, 18°W-30°E), North Atlantic Ocean, (0°-40°N, 10°-80°W), Southern  
22 Africa (0°-35°S, 8°-35°E), South Atlantic (0°-35°S, 40°W-20°E), South America (0°-35°S, 35°W-80°W), Europe (35°-65°N,  
23 10°W-50°E), East Asia (20°-48°N, 100°-140°E), Eastern USA (25°-48°N, 68°-95°W), and Western USA (25°- 48°N, 95°-  
24 125°W).

25 **Figure 14.** Tropospheric column sums of OC (<1.0 μm diameter) for (a) ATom-1 DC-8 observations; and (b) GEFS-  
26 Aerosols.

27 **Figure 15.** Tropospheric column sums of dust (<3.0 μm diameter) for (a) ATom-1 DC-8 observations; (b) GEFS-Aerosols;  
28 and (c) NGACv2.

29 **Figure 16.** Vertically resolved statistical comparisons of median values (black line is ATom-1 observation, red line is GEFS-  
30 Aerosols), r-coefficient, and median ratio (model/observation) for OC, BC and sulfate along the ATom-1 DC-8 flight tracks  
31 over the Pacific (July 29-August 8) and Atlantic (August 15-23).

- 1 **Figure 17.** Vertically resolved statistical comparisons of median values (black line is ATom-1 observation, red line is GEFS-  
2 Aerosols, green line is NGACv2), r-coefficient, and median ratio (model/observation) for dust and sea salt along the ATom-  
3 1 DC-8 flight tracks over the Pacific (July 29-August 8) and Atlantic (August 15-23).
- 4 **Figure 18.** Height-latitude profiles of OC, BC and sulfate over Atlantic on August 15 and 17<sup>th</sup>, 2016 for (a) the ATom-1 DC-  
5 8 observations; (b) GEFS-Aerosols.
- 6 **Figure 19.** Height-latitude profiles of dust (<3.0  $\mu\text{m}$  diameter) and sea salt (<3.0  $\mu\text{m}$  diameter) over Atlantic on August 15  
7 and 17<sup>th</sup>, 2016 for (a) the ATom-1 DC-8 observations; (b) GEFS-Aerosols and (c) NGACv2.

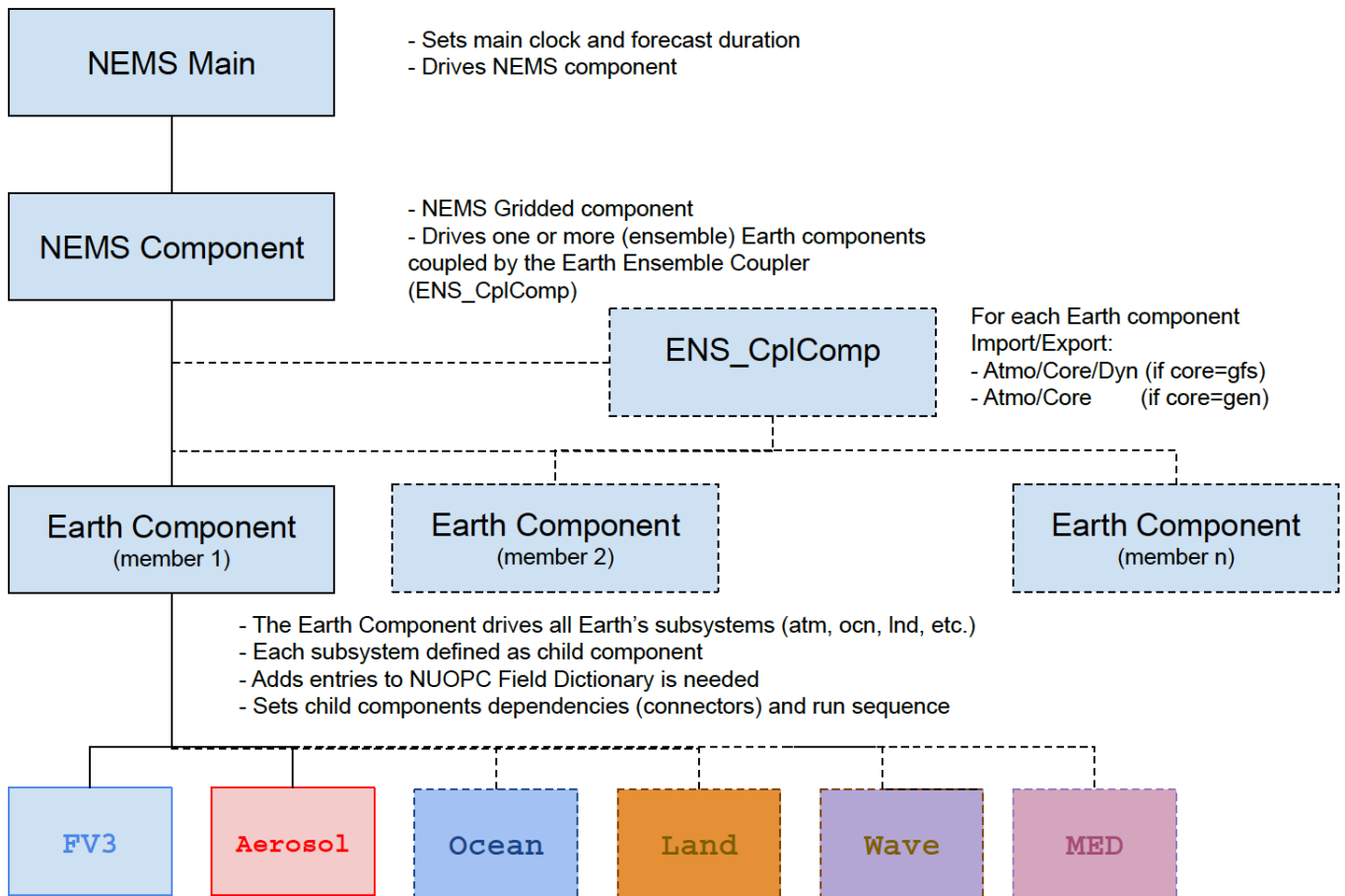


Figure 1. Diagram showing the components within the NEMS infrastructure.

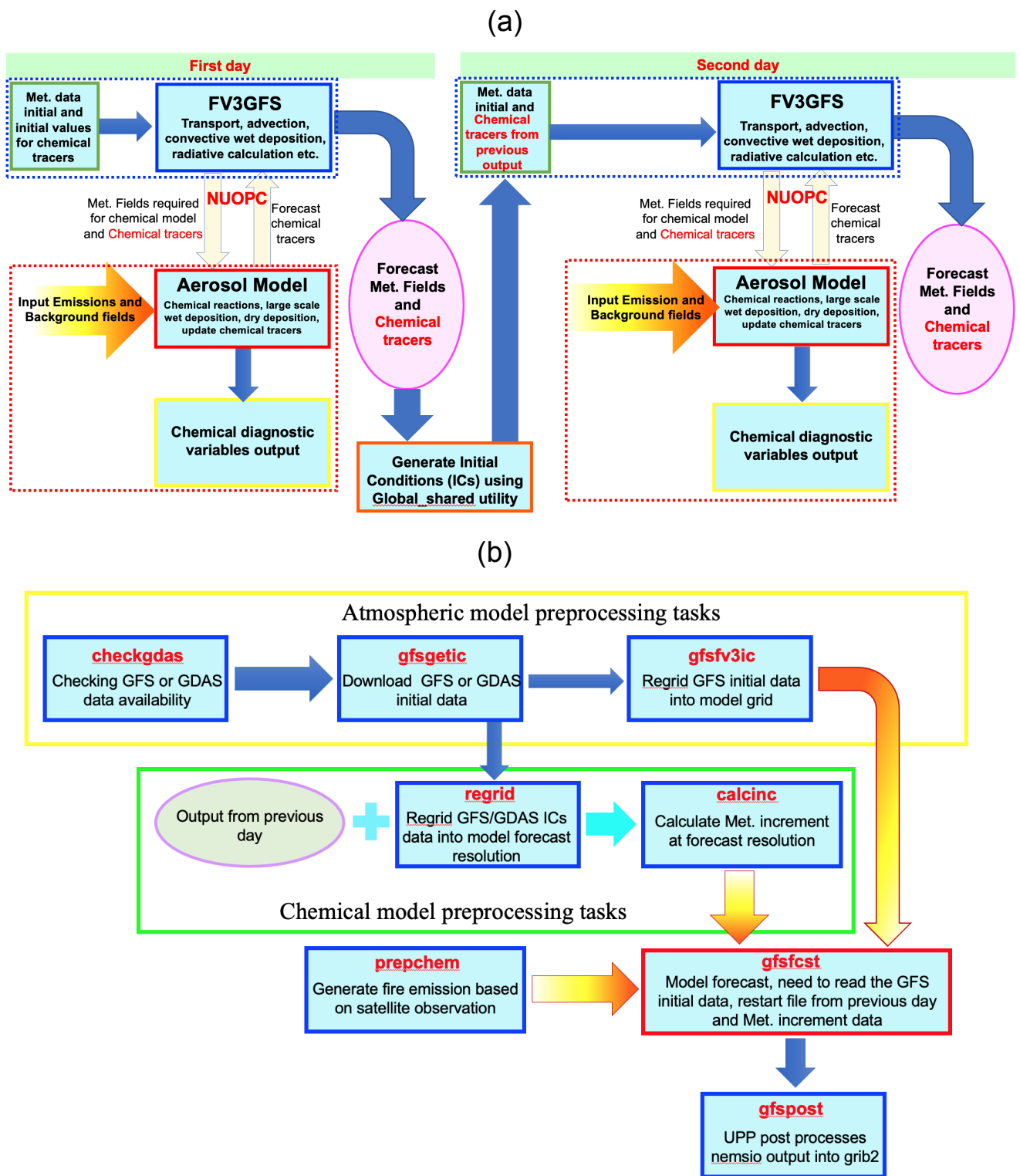


Figure 2. (a) Diagram of GEFS-Aerosols coupled structure; (b) Flowchart of steps/tasks for GEFS-Aerosols in the global workflow forecast system.

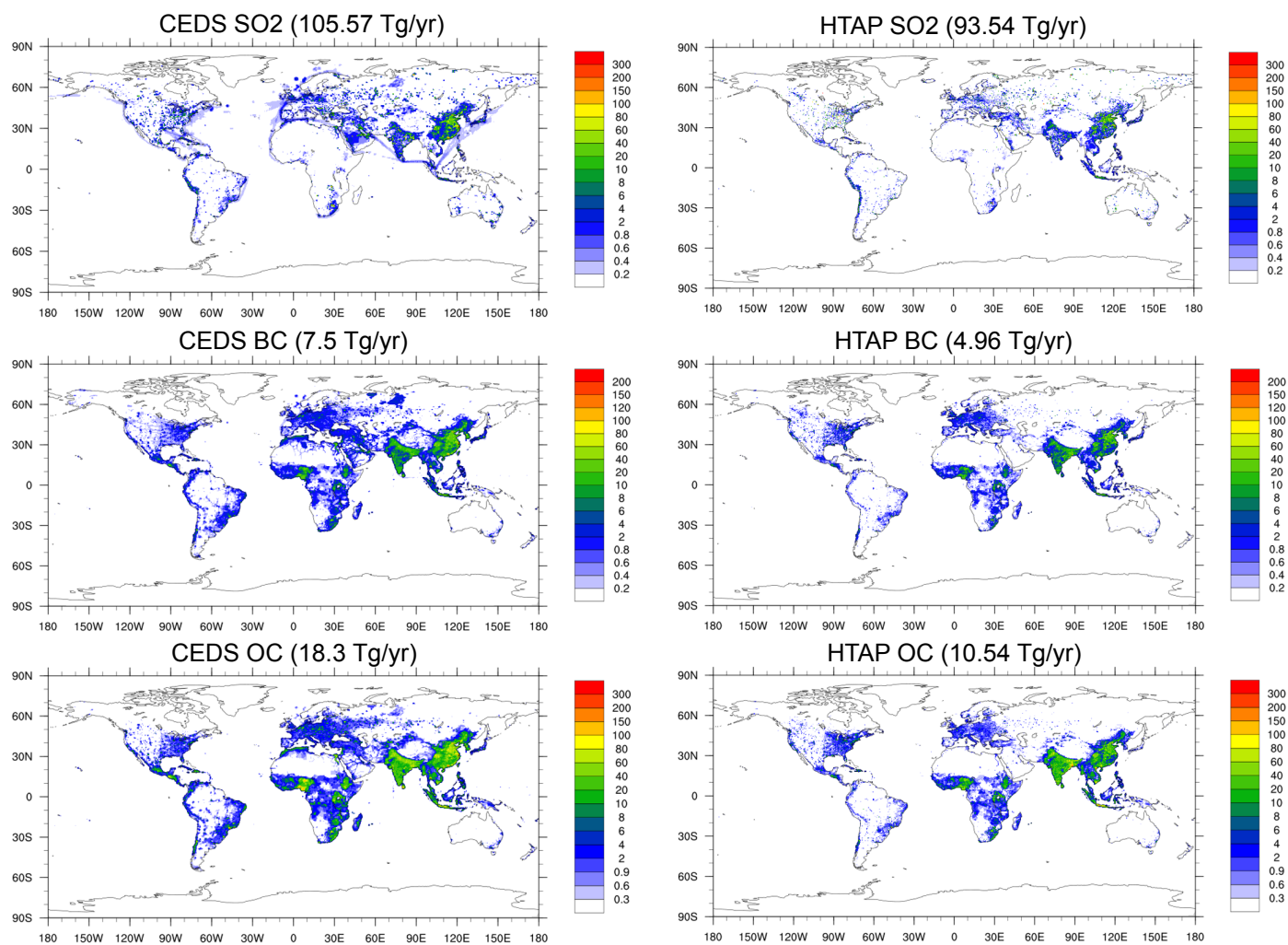


Figure 3. Anthropogenic emissions of CEDS (2014) and HTAP (2010) for SO<sub>2</sub> (mole/km<sup>2</sup>/hr), BC and OC (ng/m<sup>2</sup>/s) on summer of July.

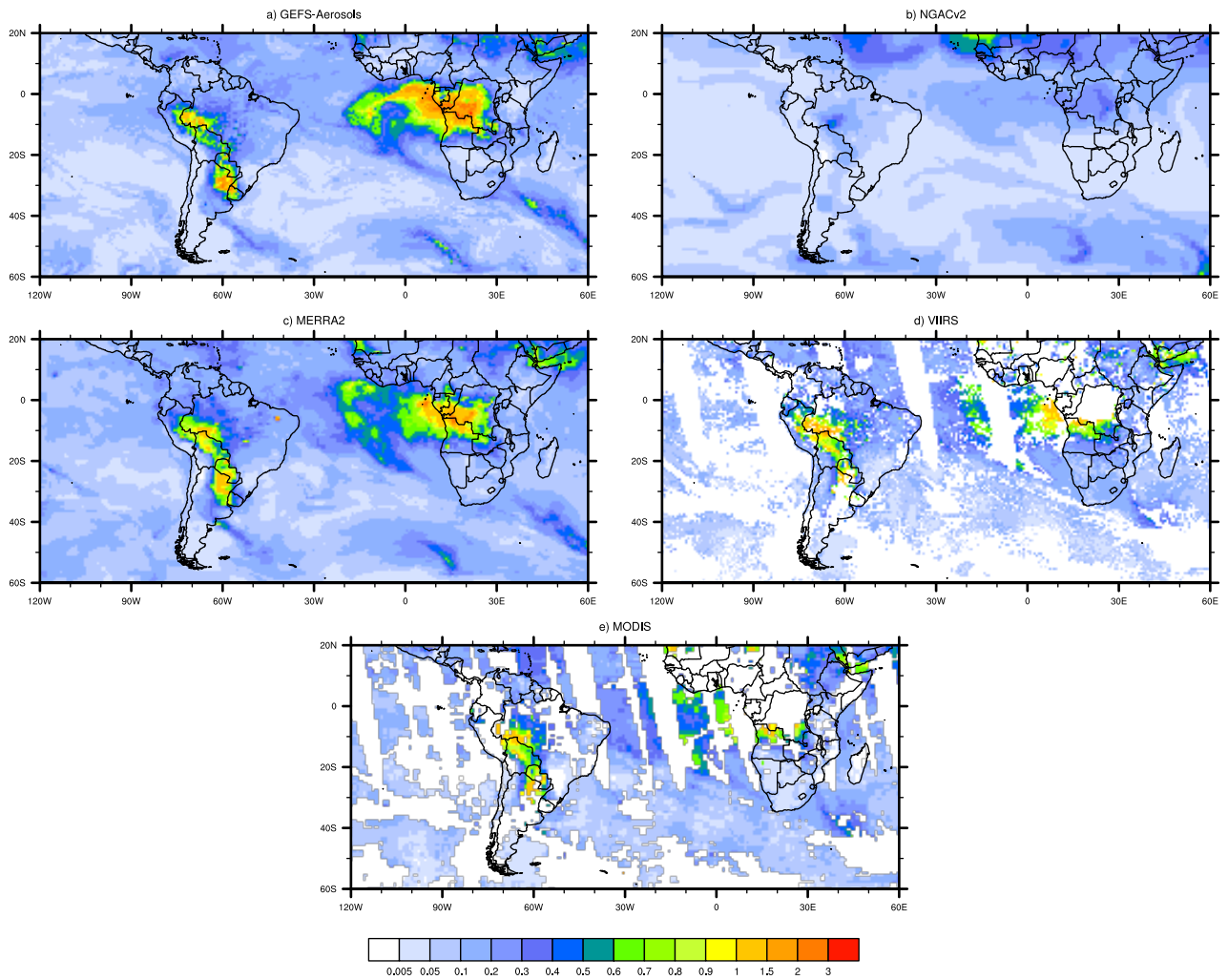


Figure 4. Total AOD forecast on 25th August verified against the NGACv2 model, MERRA2 reanalysis data and satellite observations of VIIRS and MODIS. The 18z forecasts from both models for that day and daily satellite data are used in the figure. Satellite data gaps are in white.



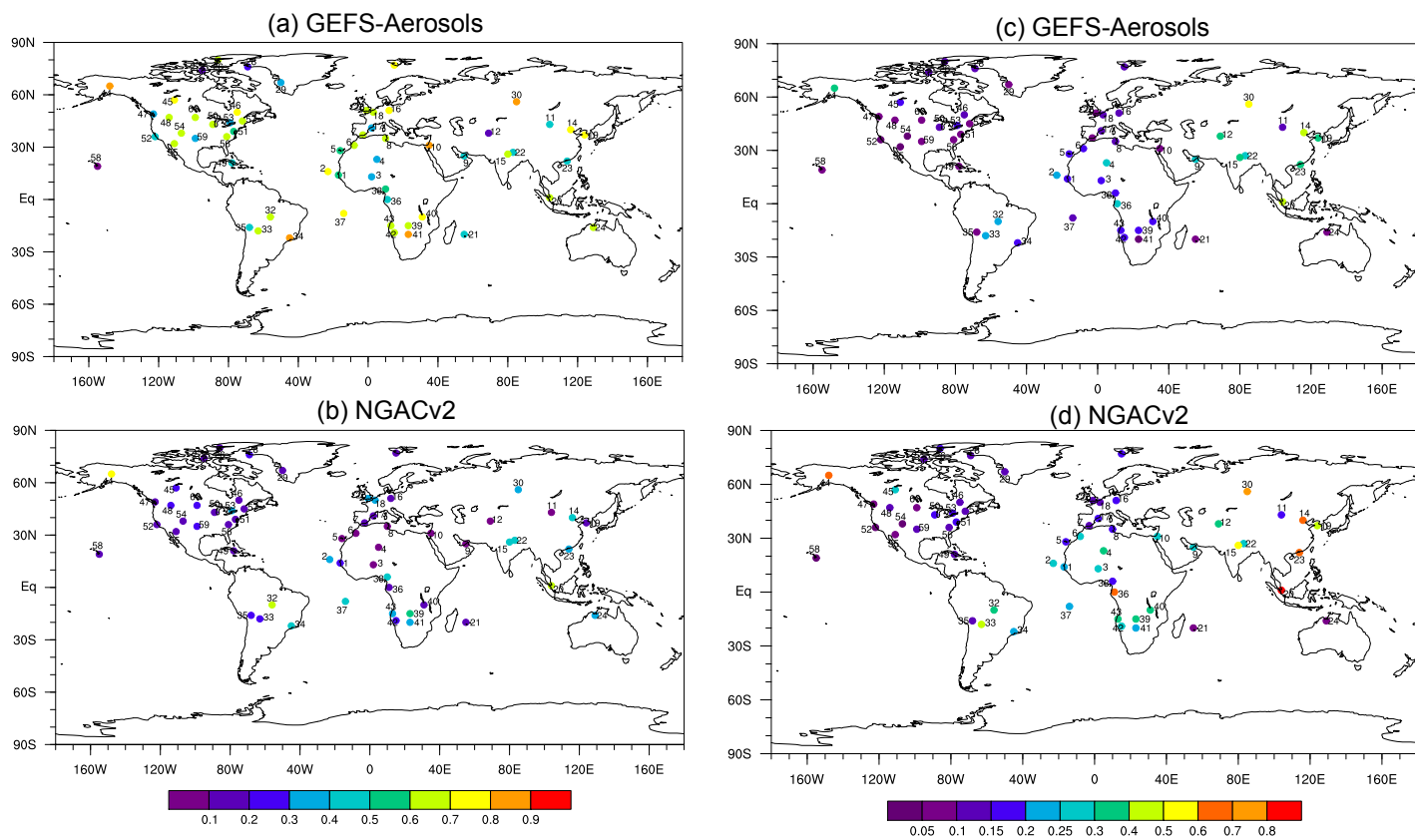


Figure 5. Correlation coefficients and RMSE between AERONET daily total AOD observations and model predictions by GEFS-Aerosols and NGACv2 for the period 7/5/19-11/30/19. Correlation coefficients are at the 95% confidence interval.

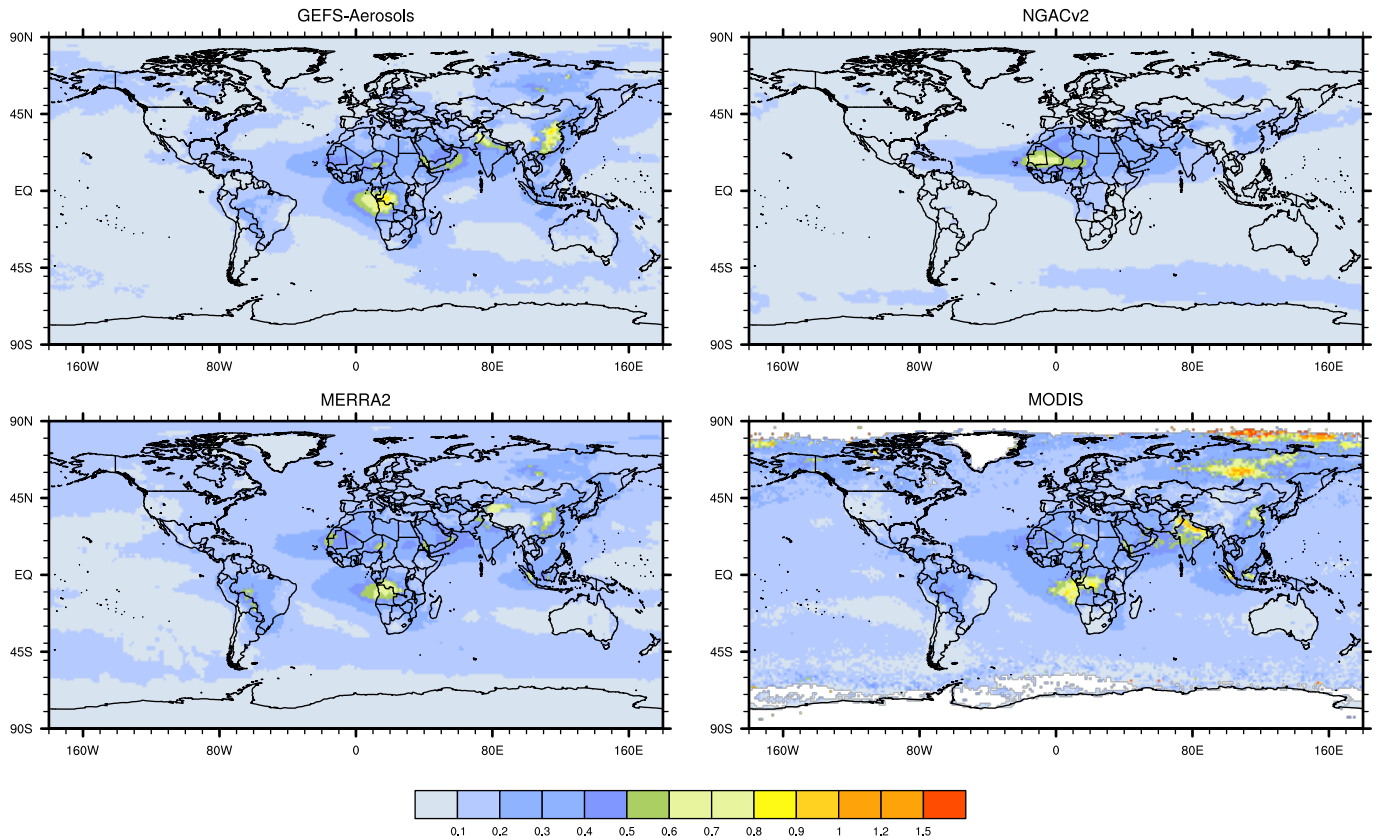


Figure 6. Day 1 AOD prediction of GEFS-Aerosols and NGACv2 compared with MERRA-2 reanalysis and MODIS averaged during 7/5/19-11/30/19.

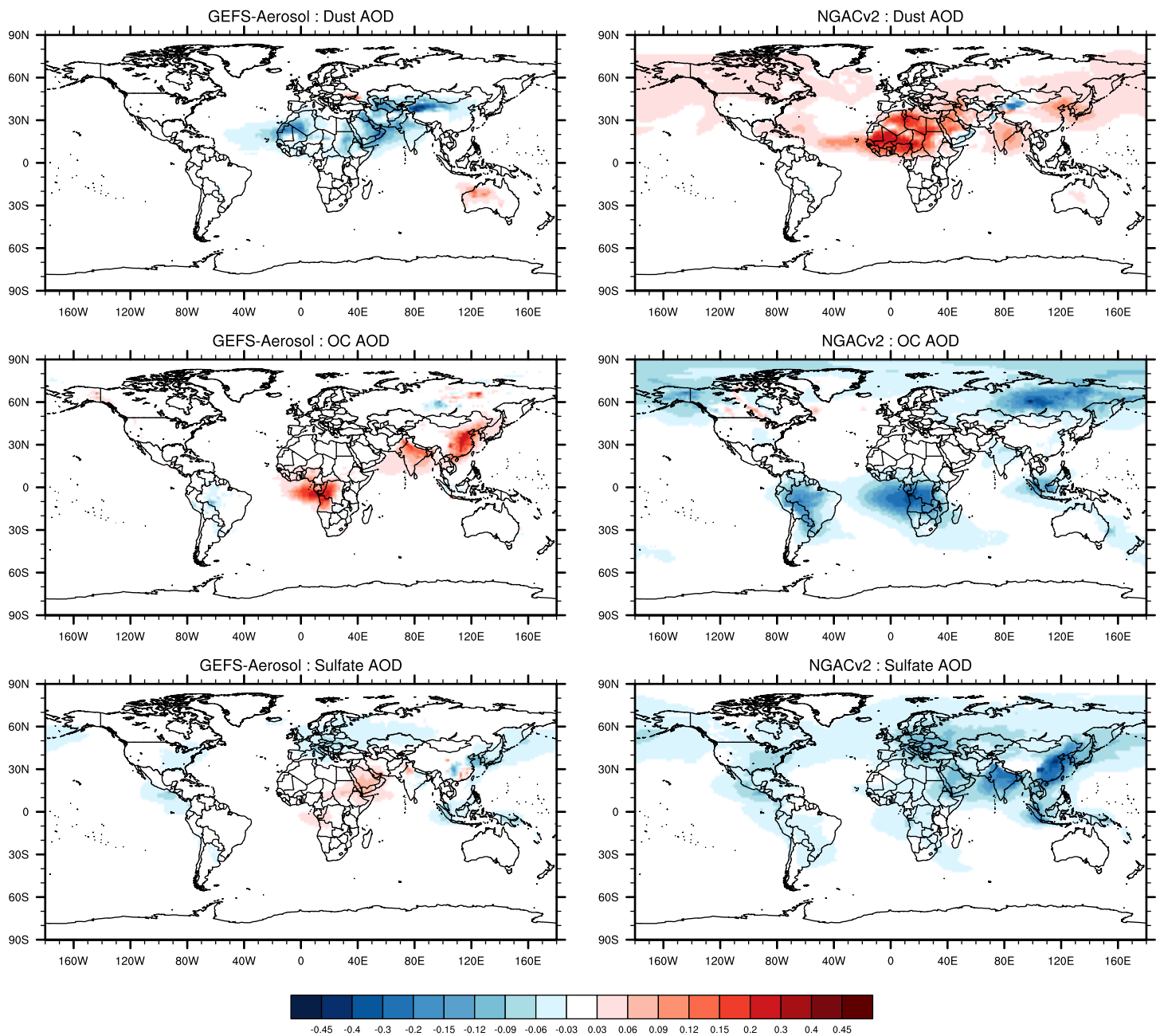


Figure 7. Day 1 AOD forecast biases of GEFS-Aerosols and NGACv2 compared with MERRA-2 averaged during 7/5/19-11/30/19 for dust, OC and sulfate.

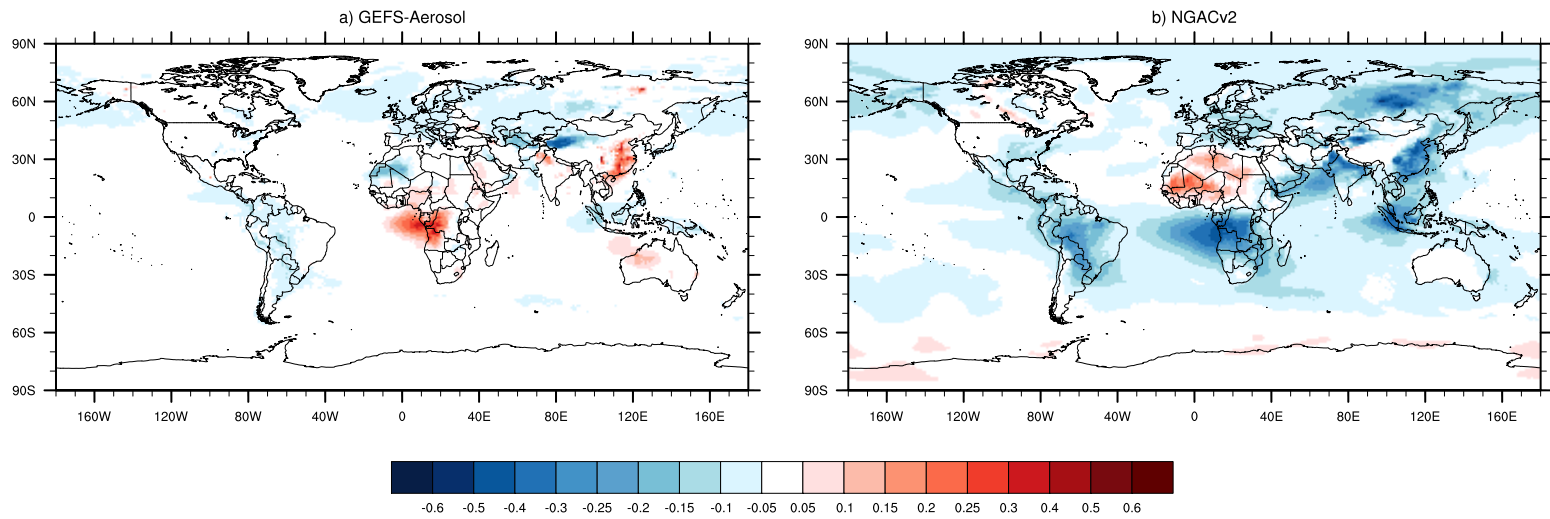


Figure 8. Differences of GEFS-Aerosols and NGACv2 Day 1 predictions of total AOD compared with MERRA-2 reanalysis averaged during 7/5/19-11/30/19.

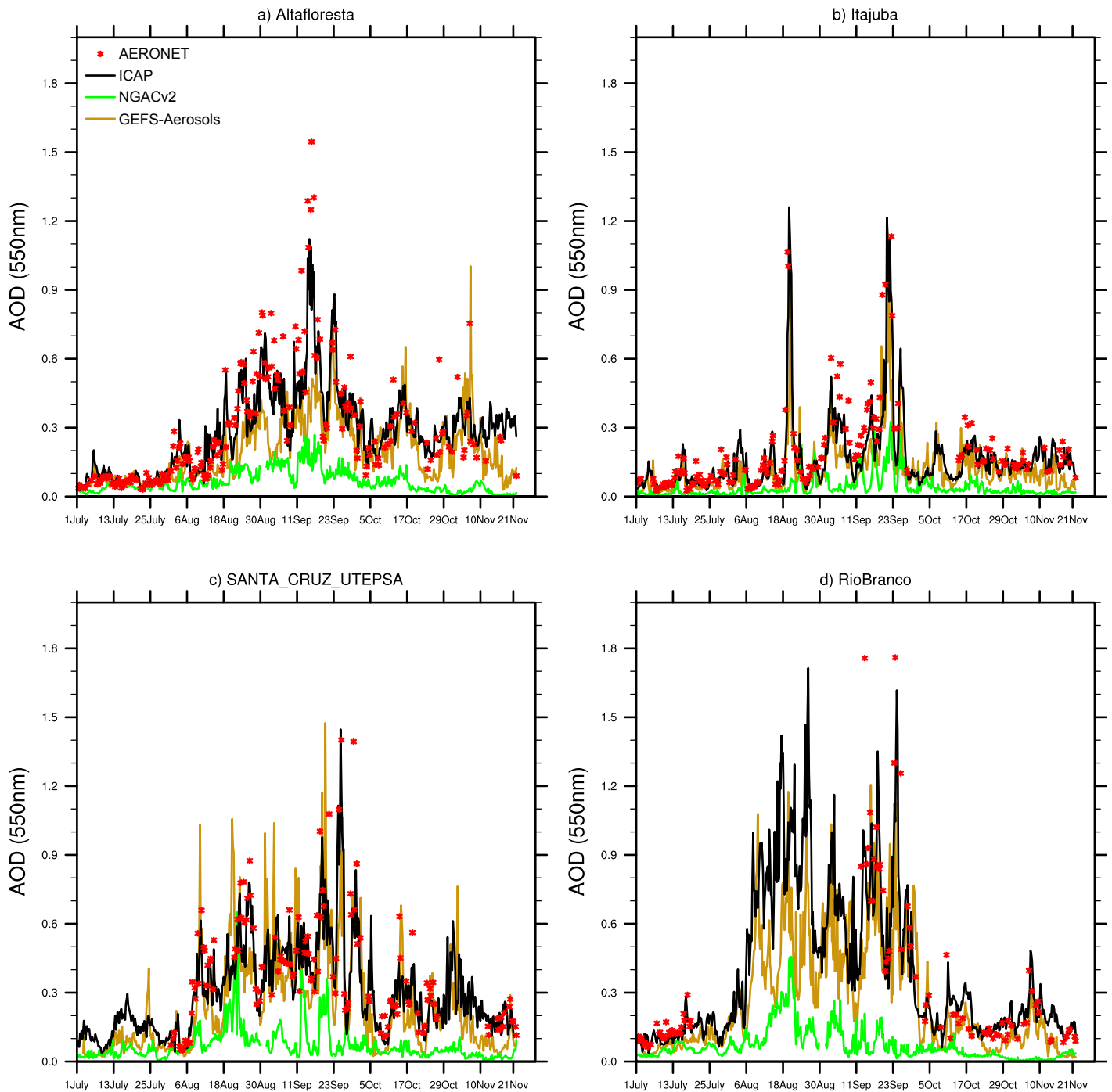


Figure 9. Day 1 AOD forecasts of GEFS-Aerosols, ICAP, and NGACv2 verified against AERONET sites in South America during 7/5/19-11/30/19.

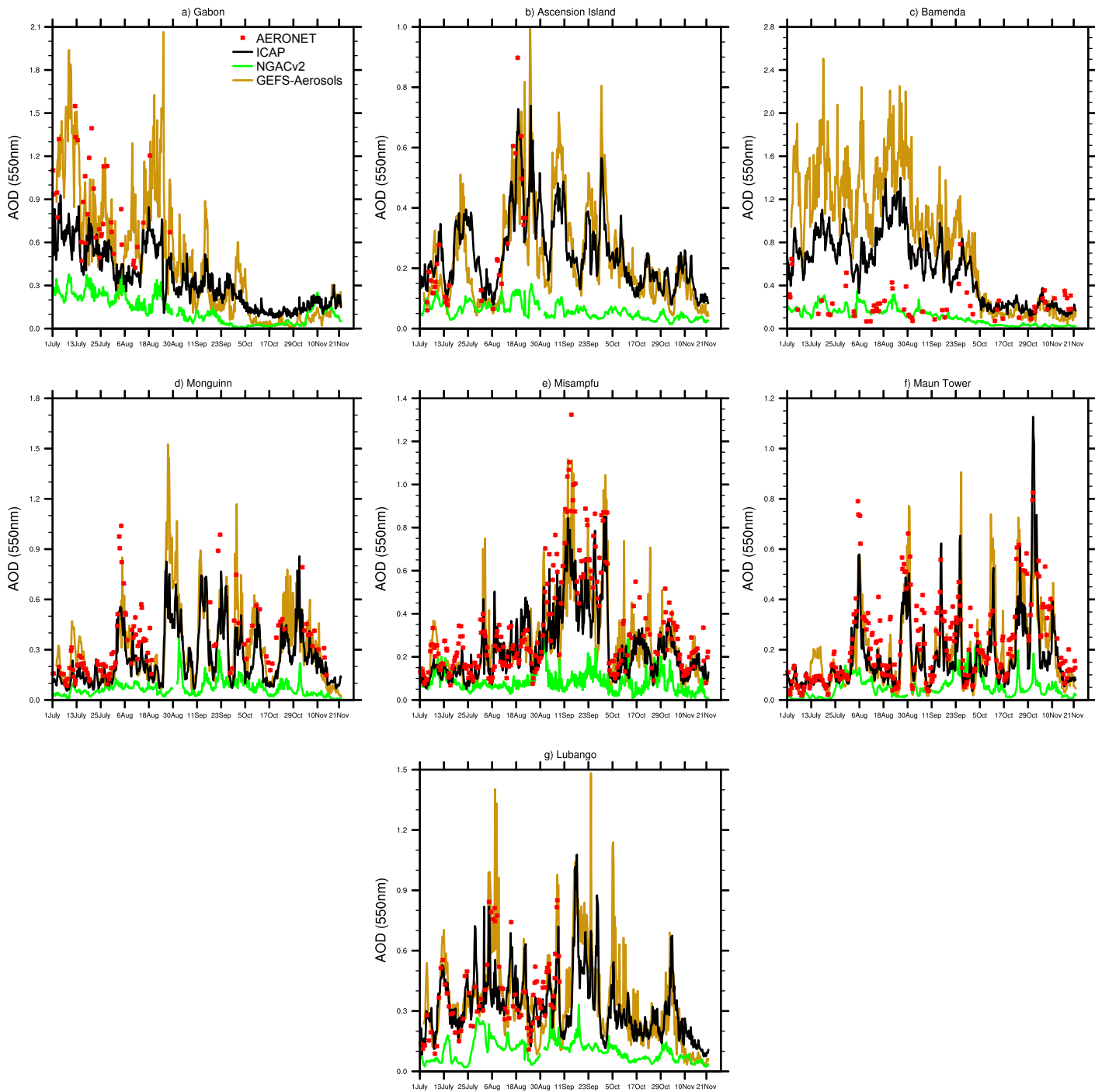


Figure 10. Day 1 AOD forecasts of GEFS-Aerosols, ICAP, and NGACv2 verified against AERONET sites in Africa during 7/5/19-11/30/19.

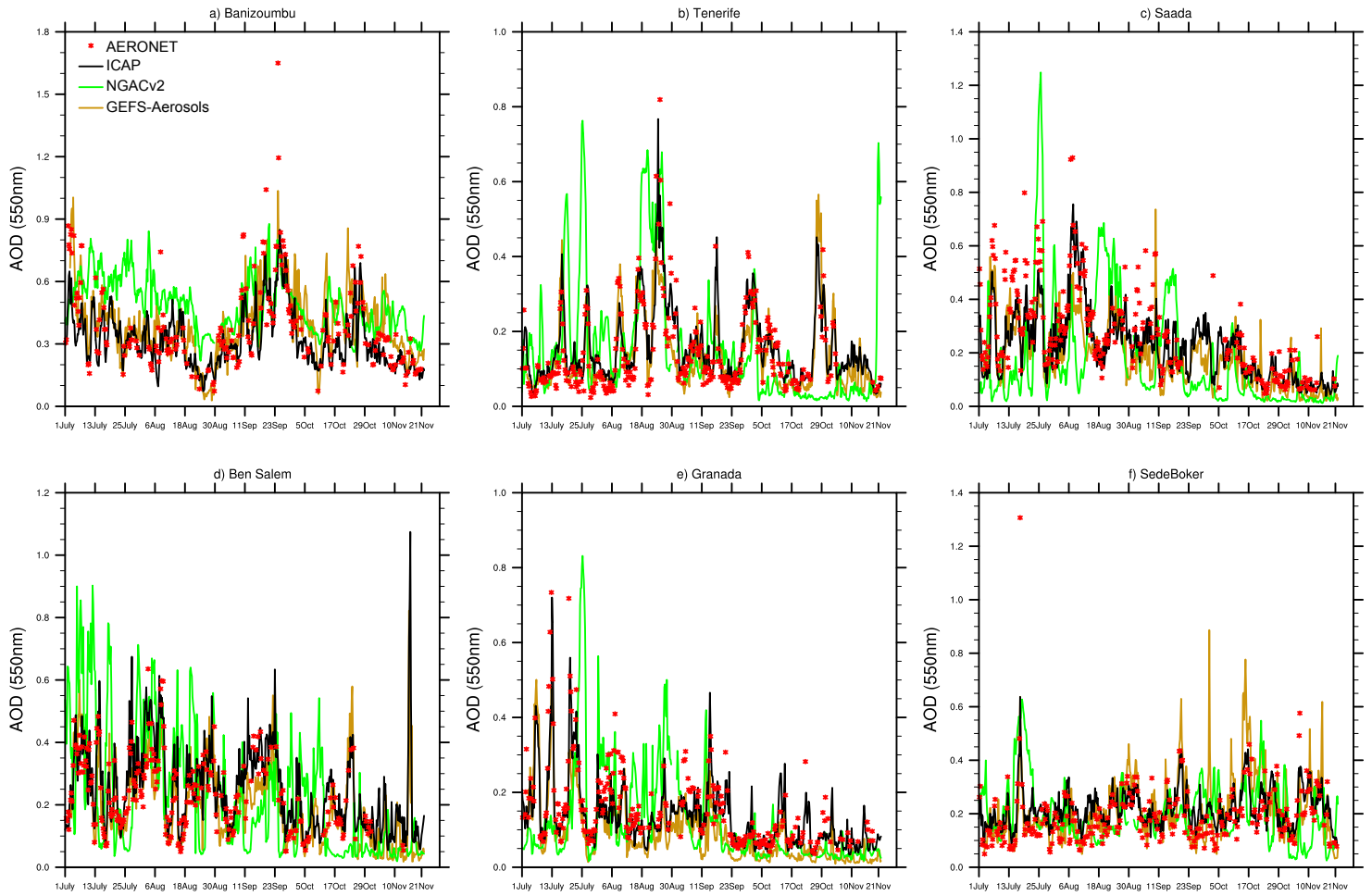


Figure 11. Day 1 AOD forecasts of GEFS-Aerosols, ICAP, and NGACv2 verified against AERONET sites in dust source regions and surrounding downwind areas during 7/5/19-11/30/19.

## AERONET Stations



• GEFS-Aerosols

• NGACv2

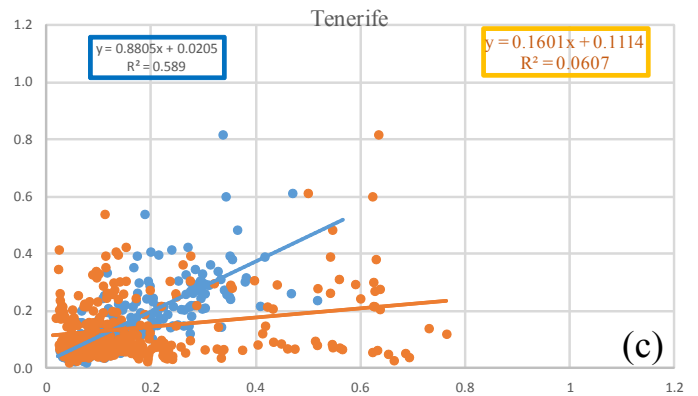
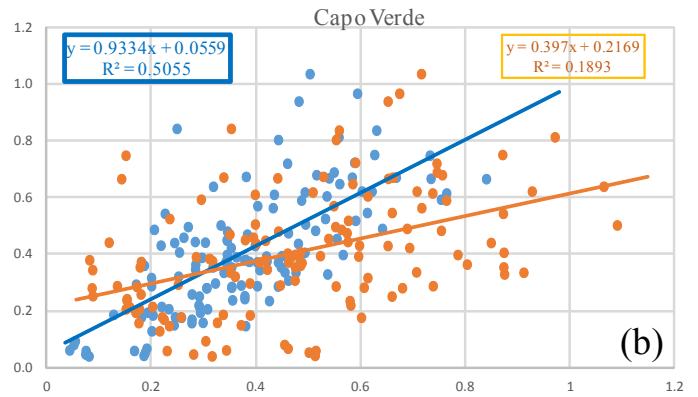
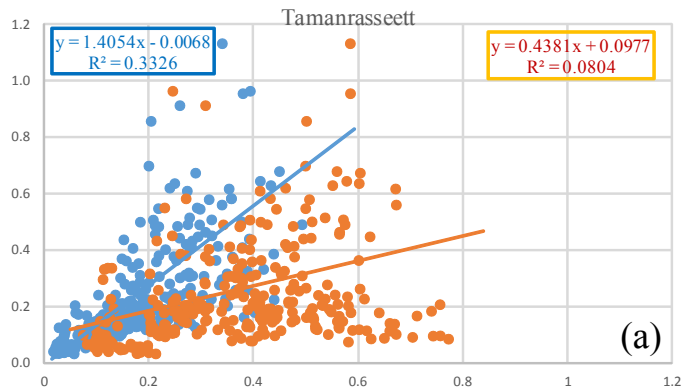


Figure 12. Daily AERONET total AOD versus modeled total AOD from GEFS-Aerosols (blue) and NGACv2 (orange) at the AERONET sites of (a) Tamanrasset, (b) Cape Verde, and (c) Tenerife with linear regression fits.



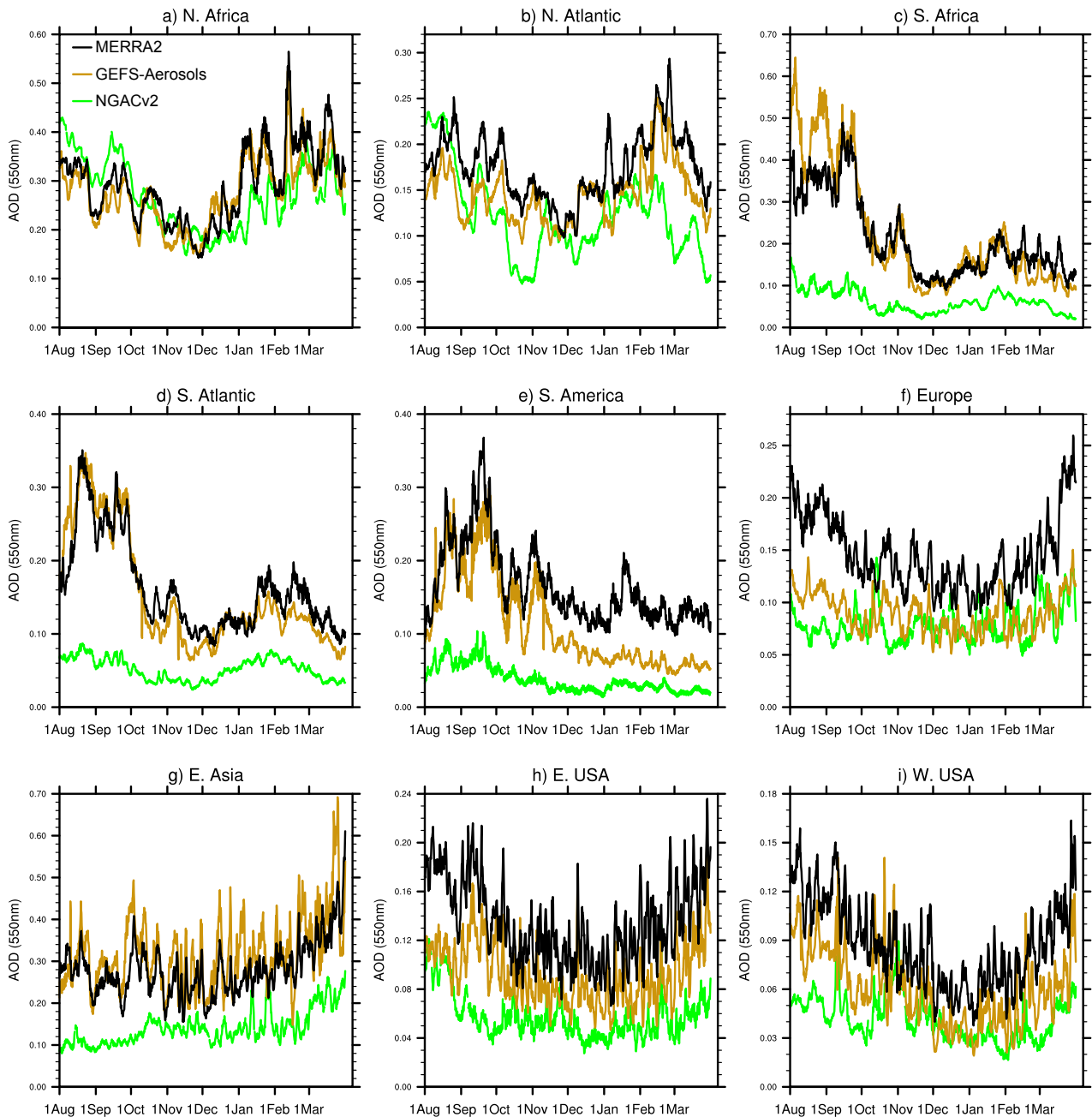


Figure 13. GEFS-Aerosols and NGACv2 day 1 total AOD forecast time series against MERRA-2 reanalysis data averaged over major global regions of North Africa ( $0^{\circ}$ - $35^{\circ}$ N,  $18^{\circ}$ W- $30^{\circ}$ E), North Atlantic Ocean, ( $0^{\circ}$ - $40^{\circ}$ N,  $10^{\circ}$ - $80^{\circ}$ W), Southern Africa ( $0^{\circ}$ - $35^{\circ}$ S,  $8^{\circ}$ - $35^{\circ}$ E), South Atlantic ( $0^{\circ}$ - $35^{\circ}$ S,  $40^{\circ}$ W- $20^{\circ}$ E), South America ( $0^{\circ}$ - $35^{\circ}$ S,  $35^{\circ}$ W- $80^{\circ}$ W), Europe ( $35^{\circ}$ - $65^{\circ}$ N,  $10^{\circ}$ W- $50^{\circ}$ E), East Asia ( $20^{\circ}$ - $48^{\circ}$ N,  $100^{\circ}$ - $140^{\circ}$ E), Eastern USA ( $25^{\circ}$ - $48^{\circ}$ N,  $68^{\circ}$ - $95^{\circ}$ W), and Western USA ( $25^{\circ}$ - $48^{\circ}$ N,  $95^{\circ}$ - $125^{\circ}$ W).

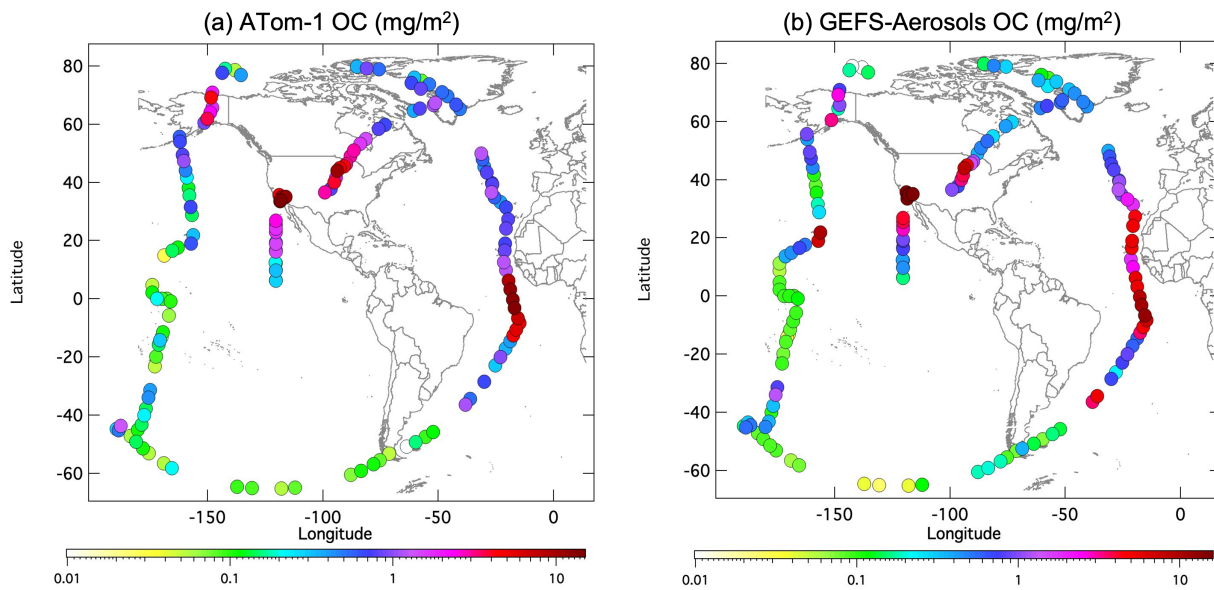


Figure 14. Tropospheric column sums of OC (<1.0 μm diameter) for (a) ATom-1 DC-8 observations; and (b) GEFS-Aerosols.

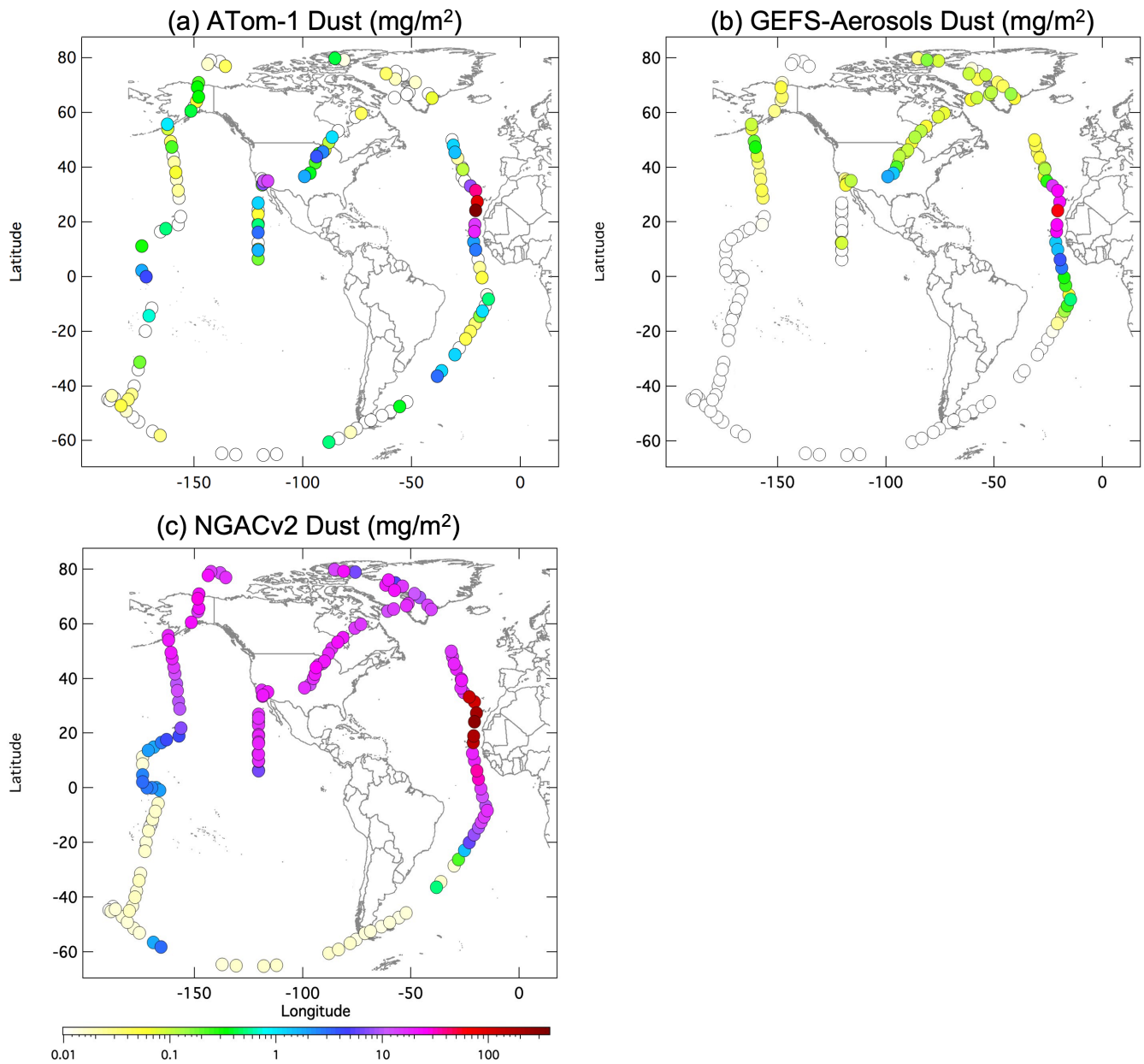


Figure 15. Tropospheric column sums of dust (<math><3.0 \mu\text{m}</math> diameter) for (a) ATom-1 DC-8 observations; (b) GEFS-Aerosols; and (c) NGACv2.

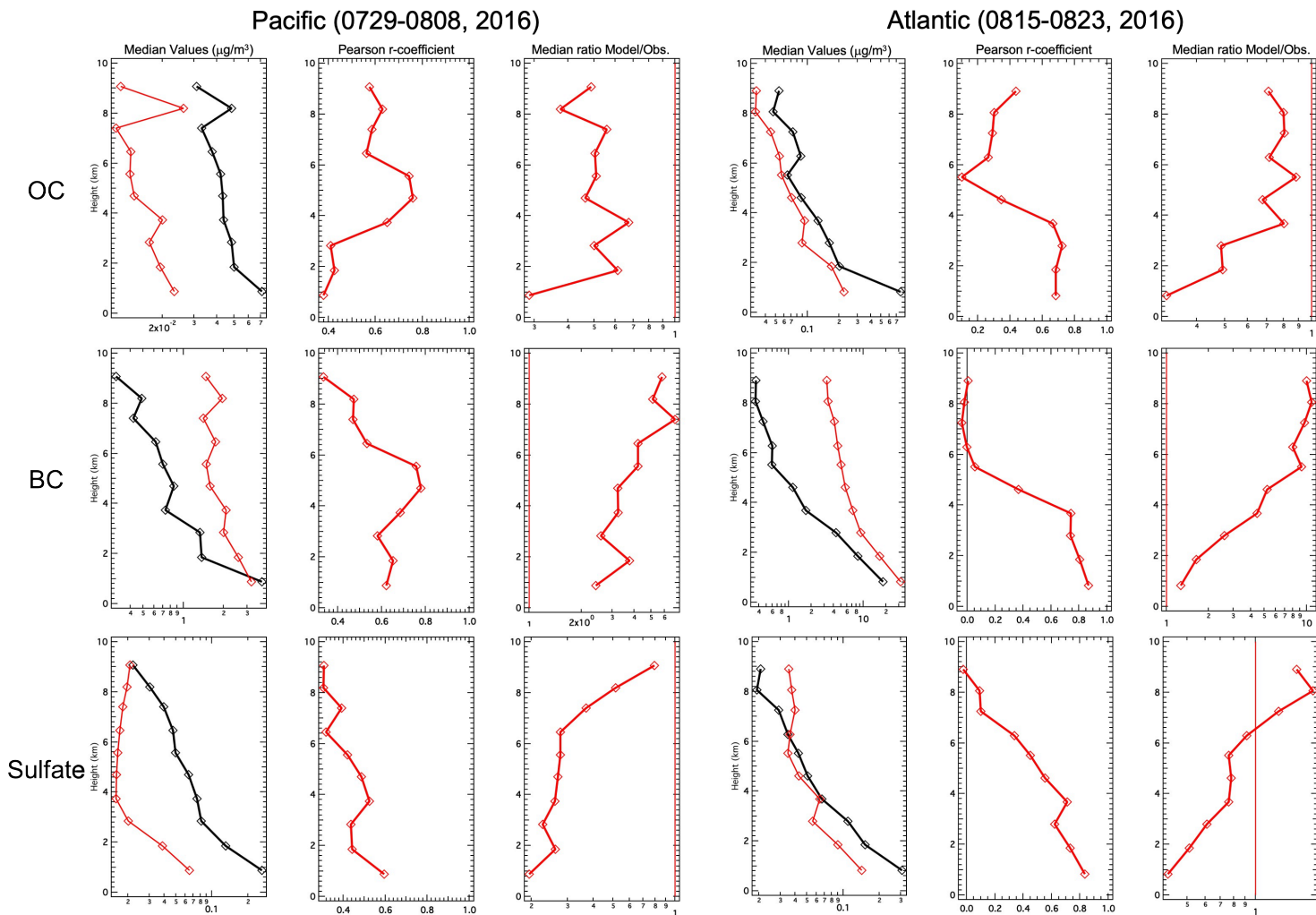


Figure 16. Vertically resolved statistical comparisons of median values (black line is ATom-1 observation, red line is GEFS-Aerosols), r-coefficient, and median ratio (model/observation) for OC, BC and sulfate along the ATom-1 DC-8 flight tracks over the Pacific (July 29-August 8) and Atlantic (August 15-23).

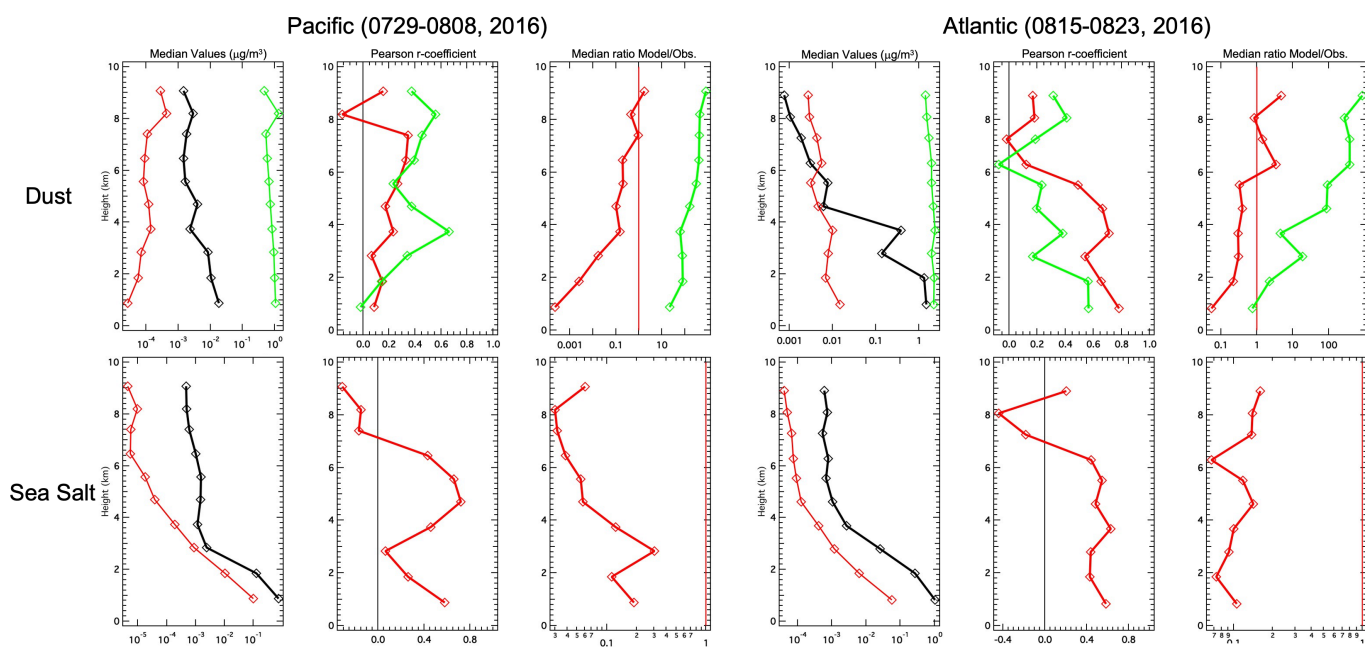


Figure 17. Vertically resolved statistical comparisons of median values (black line is ATom-1 observation, red line is GEFS-Aerosols, green line is NGACv2), r-coefficient, and median ratio (model/observation) for dust and sea salt along the ATom-1 DC-8 flight tracks over the Pacific (July 29-August 8) and Atlantic (August 15-23).

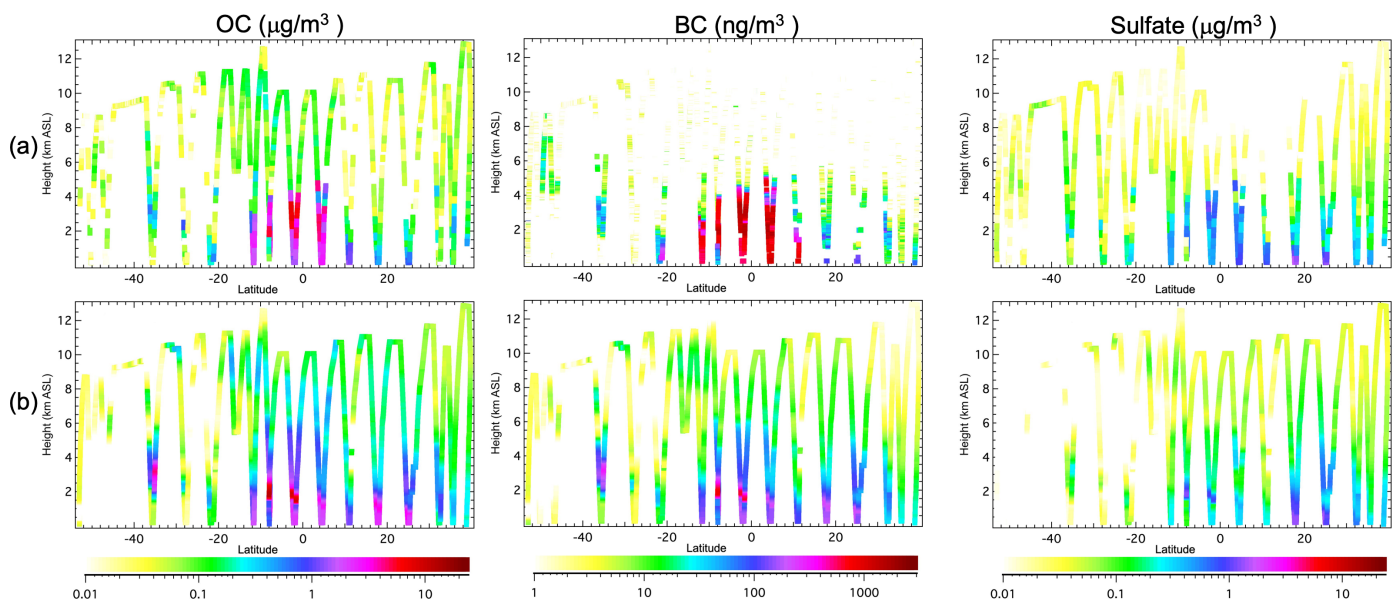


Figure 18. Height-latitude profiles of OC, BC and sulfate over Atlantic on August 15 and 17th, 2016 for (a) the ATom-1 DC-8 observations; (b) GEFS-Aerosols.

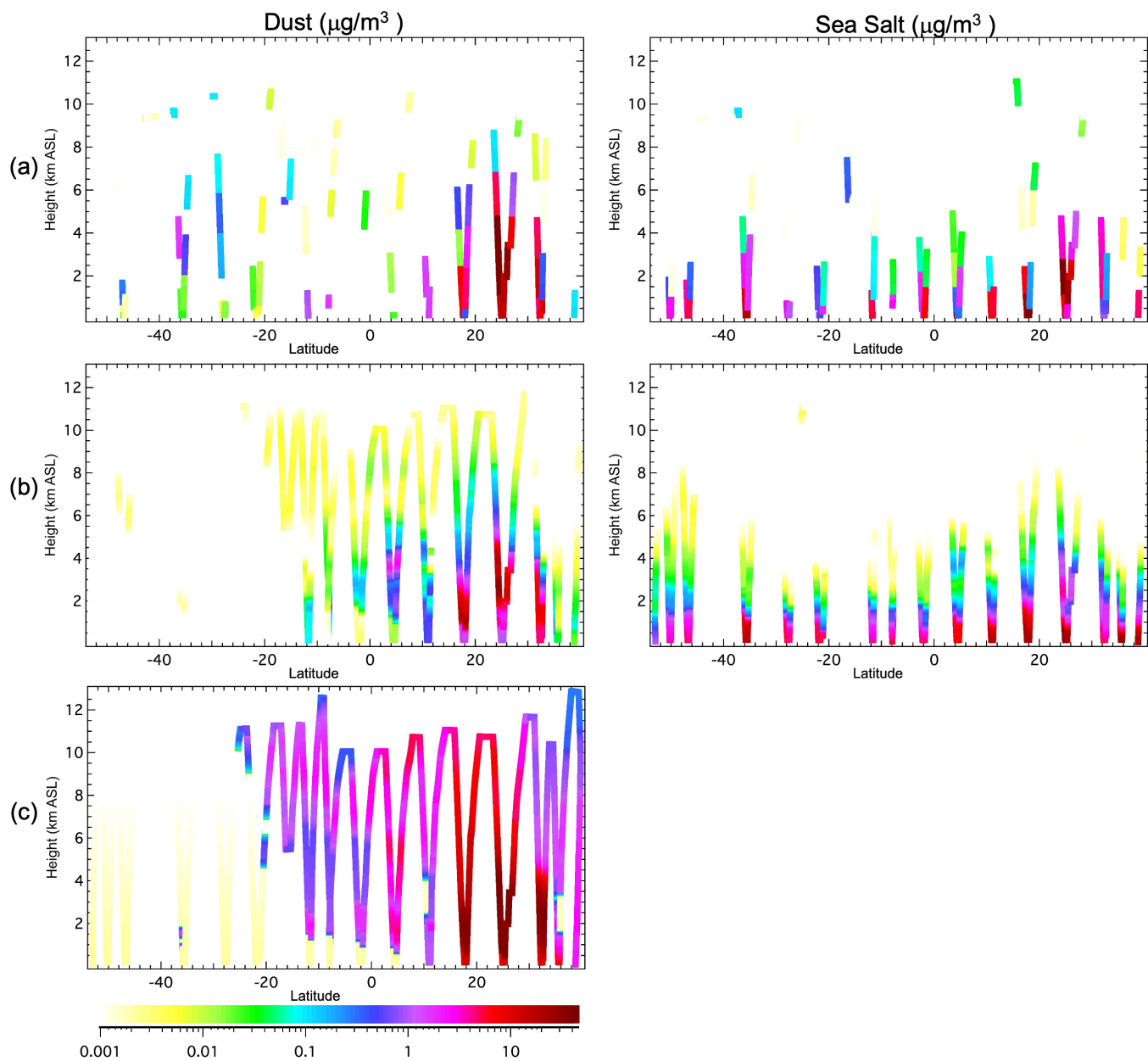


Figure 19. Height-latitude profiles of dust ( $<3.0 \mu\text{m}$  diameter) and sea salt ( $<3.0 \mu\text{m}$  diameter) over Atlantic on August 15 and 17th, 2016 for (a) the ATom-1 DC-8 observations; (b) GEFS-Aerosols and (c) NGACv2.